THE UNIVERSITY OF QUEENSLAND

Preliminary Assessment of the Level of Vulnerability of Queensland's Transmission Network to Geomagnetically Induced Currents

by

Edward Burstinghaus

The School of Information Technology and

Electrical Engineering

The University of Queensland

Submitted for the degree of

Bachelor of Engineering (Honours)

in the division of Electrical Engineering

November 2012.

Edward Burstinghaus
41772092
PO Box 3102
Tarragindi 4121 QLD

November 1, 2012

Prof Paul Strooper
Head of School
School of Information Technology and Electrical Engineering
The University of Queensland
St Lucia QLD 4072

Dear Professor Strooper,

In accordance with the requirements of the degree of Bachelor of Engineering (Honours) in the division of Electrical and Electronic Engineering, I present the following thesis entitled "Preliminary Assessment of the Level of Vulnerability of Queensland's Transmission Network to Geomagnetically Induced Currents". This work was performed [with the support of Powerlink Queensland] under the supervision of Professor Tapan Saha.

I declare that the work submitted in this thesis is my own, except as acknowledged in the text and footnotes, and has not been previously submitted for a degree at the University of Queensland or any other institution.

Yours sincerely,

Edward Burstinghaus

To Paul and Elisabeth

Acknowledgments

I have many people to thank for their help, much of which was crucial help, throughout this project. I would like to thank my University supervisor Professor Tapan Saha for supporting me throughout the project even though the topic was somewhat unusual. Discussions with him always ensured that I had my main goals in mind and was on track to complete the project on time. Though I only used the educational version of PowerWorld Simulator in the end, I still appreciate his guidance in my use of this software as it confirmed the validity of my results.

I would like to thank Michael Hocker, my supervisor at Powerlink Queensland. His technical advice for me as an experienced power engineer was oftentimes invaluable. Among several other things he advised me on how to acquire the network parameters from a PSS/E casefile, whom to seek within Powerlink to acquire other forms of information and some of the finer points of the limitations of the final results of my project. Help from several other individuals within Powerlink as well as the Spatial Data Team has also been greatly appreciated and was crucial in my acquiring data which correctly represents the Queensland power transmission network. I also greatly appreciate the support of the Australian Power Institute, without which I would not have been privileged with experience in the power industry while at an undergraduate level.

I would like to thank Associate Professor Colin Waters and Doctor Murray Sciffer of the Centre for Space Physics at the University of Newcastle. They both guided me in my attempt to implement a complex, spectral domain surface impedance method which they had used in one of their publications to model geoelectromagnetic induction in one dimension. Though my attempt to use this method failed and I instead resorted to a simpler, temporal domain, finite-difference method, I compared my results using the latter method with those of the former to verify the correct order of magnitude of the geoelectric field estimations. I also believe that their help motivated me to better understand the phenomenon of induction in an Earth of layered conductivity and this was crucial in understanding the limitations of the final results. Also of no small significance was the help of Richard Marshall of the

Ionospheric Prediction Service. The idea to investigate GIC distributions in the Queensland power transmission network, which preceded all of my ideas for this project, is attributable to him in the first place. He also advised me several times on sources for geomagnetic data and on general principles of space physics.

I was delightfully surprised at the willingness of the international space physics community to help me in this project despite my being merely an undergraduate student of electrical engineering and physics. I would like to thank Risto Pirjola of the Finnish Meteorological Institute for crucial help in calculating distributions of GICs in power systems given known geoelectric fields. His help with my understanding of the geomagnetic coastal effect is also greatly appreciated. I would like to thank Tohru Araki and Doctor Bruce Tsurutani; both space weather scientists who gave me essential help in my understanding of space weather disturbances in general and Sudden Commencements in particular. I must also thank the Ionospheric Prediction Service for the provision of geomagnetic data and Geoscience Australia for the provision of papers and reports on magnetotelluric surveys.

Finally I would like to thank Professor Kiyohumi Yumoto of Kyushu University in Japan and the International Centre for Space Weather Science and Education for provision of geomagnetic data on which one of the most important results of this project is based.

Abstract

Geomagnetic disturbances can generate Geomagnetically Induced Currents (GICs) in power transmission networks, which can cause voltage stability issues and transformer damage. Though it has historically been assumed that this issue was only relevant for countries at high latitudes, research during recent years has shown that this may not be the case. In particular, an event known as a geomagnetic Sudden Commencement (SC) has been linked with significant GICs in mid and low-latitude regions. To help ascertain which transformers in their network are most vulnerable to GICs, power utilities will need software tools to estimate distributions of these currents in their systems. Such tools are currently being built into several commercial power system software packages. To use this software however, utilities will also need methodologies by which to estimate the non-uniform geoelectric fields which are likely to be induced in their region during geomagnetic disturbances. In this thesis a methodology is developed for estimating GIC distributions in a power network using temporal geomagnetic data collected at multiple magnetic observatories. It is also demonstrated that significant error in the distribution of GICs calculated for a given event is likely to occur if a simpler uniform geoelectric field is used instead of a more realistic non-uniform one. In particular a phenomenon known as the geomagnetic coastal effect, for which an approximate modelling technique is developed in this thesis, forces induced geoelectric fields to be highly non-uniform in the vicinity of coastlines. The estimation methodology developed is also used to estimate the GIC distribution which would occur in a particular power network in a mid-latitude region if the unique and powerful SC of March 24 1991 occurred today.

Contents

List of Figures

List of Tables

Chapter 1

Introduction

Space weather disturbances can induce quasi-DC currents in power transmission networks. These currents are known as Geomagnetically Induced Currents or GICs. Because power transformers are not designed to operate under direct current excitation, GICs can cause them to become half-cycle saturated. In such a state power transformers consume increased amounts of reactive power and inject significant harmonic currents into the system. If the space weather disturbance is severe enough this can lead to miss-operation of power system protection, voltage instability or even voltage collapse of the network. It is also a point debated in the literature that operation under half-cycle saturation can damage power transformers via overheating of components exposed to significant stray flux.

Space weather has traditionally not been investigated in such low latitude regions as Queensland due to it not having been linked to any major system disturbances in a region so far from the geomagnetic poles of the planet. In fact, no disturbance in any Australian power network has ever been found to have been caused by space weather. Recent findings however have raised the concern that there may be rare events which could have significant consequences for power systems at all latitudes. It has also been posed recently that GICs can cause significant degradation to power transformer winding insulation which accelerates their eventual failure some months or years later, instead of causing any immediate issues. Combined with the fact that power systems become more vulnerable to space weather as their transmission capacity increases, these findings have led to the need to re-evaluate the risk posed to Australian power transmission networks by space weather disturbances. A secondary aim of this thesis was to assist Powerlink Queensland in that re-evaluation. Powerlink Queensland is the owner and operator of the Queensland power transmission network and their system in particular was studied in the works of this thesis. The results of this project are however applicable to all power networks on Earth and the network belonging to Powerlink Queensland is not considered uniquely vulnerable to space weather in any way. This organisation will herein be referred to as simply PLQ.

The primary aims of this thesis were:

- to develop a methodology by which to estimate GIC distributions in a power network using estimates of non-uniform geoelectric fields
- to investigate the importance of non-uniform geoelectric fields, as opposed to uniform ones, in estimating GIC distributions in power networks
- to try and predict the worst-case GICs which could be generated in the Queensland power transmission network

Chapter 2 gives an overview of the theory which was used to develop the GIC estimation methodology. Much of this is related to the calculation of GICs in a power network given a specified uniform geoelectric field. The nodal admittance matrix method was implemented to perform this calculation. Following this two techniques by which to estimate geoelectric fields generated during geomagnetic disturbances are explained. Both methods use temporal geomagnetic data to estimate the geoelectric fields. Due to reasons explained in Chapter 4, only one of these methods was adopted in this project. A theoretical model for the geomagnetic coastal effect is then presented and finally the meaning of effective transformer GIC is explained.

In Chapter 3 a literature review on the impacts of space weather on power transmission networks is presented. Many topics are covered including the ionospheric current systems which cause terrestrial geomagnetic disturbances, the connection between GICs in low latitude regions and geomagnetic Sudden Commencements (SCs), a physical model for SCs, the nature of half-cycle saturation of power transformers and a general review of studies of GICs in power networks. The need for collaboration between the power engineering community and the geophysics and space physics communities to facilitate quick responses to space weather disturbances is also stressed.

In Chapter 4 the GIC estimation methodology which was developed during the project is explained in full. Several types of data pertaining to the electrical parameters and topology of the Queensland network were collected during the project. The sources of these data types and the issues encountered while collecting them are explained for each. The disassociation of the Queensland transmission networks from the distribution networks in Queensland is then explained. This was necessary because most data pertaining to the distribution networks was not available during the project as these belong to companies other than PLQ. For the same reason the New South Wales transmission network had to be disassociated from that of Queensland; this is also explained. Following this the software which was written during this project is described and also verified. Software was written to calculate GIC distributions in a power network given a uniform geoelectric field as well as a non-uniform geoelectric field, to estimate geoelectric fields using temporal geomagnetic data and to roughly model the geoemagnetic coastal effect. The sources of and methods for handling all geomagnetic data are also detailed.

The results of the project are presented in Chapter 5. The first of these are distributions of GICs in the Queensland power transmission network given uniform 1V/km northward and westward geoelectric fields. Several interesting properties of GIC distributions are investigated. Following this uniform fields are used for preliminary estimations of the GICs which were present in the measured transformer for a handful of GIC spikes which occurred in the latter half of 2012. It is found that they correlate well with the measured data but are out by a relatively consistent scaling factor. The average conductivity of the Earth beneath Queensland and the level of influence of the geomagnetic coastal effect are then scaled, using appropriate and physically justifiable constraints, so that the estimated GICs for these events match those which were measured. The Sudden Commencement of the 14th of July 2012 is then used as an example to demonstrate the difference in the distribution of GICs which result from using a simpler uniform field instead of a more realistic non-uniform one. Also, the GIC distribution which would be present in the Queensland network if the unique and powerful Sudden Commencement of March 24 1991 occurred today is estimated.

Chapter 6 discusses the limitations of the project. Several sources of potential error are discussed including the missing distribution network data, the simplistic conductivity model for Queensland, the rough and phenomenological model which is used for the geomagnetic coastal effect and the non-ideal location of the one GIC measurement device in the network. In particular the fact that two unknown physical parameters were scaled using the measurements of only one GIC measurement device is stressed as a likely source of inaccuracy of the GIC estimations. Chapter 7 is the concluding Chapter of this thesis.

In the network data recorded for the studies conducted in this thesis, data was estimated for some transmission lines, substation earth grids and transformers belonging to companies other than PLQ. These companies include power generation companies and power distribution companies in general. The GICs which were estimated to flow through the equipment belonging to these companies can be expected to be less accurate than those estimated to flow through PLQ equipment in general because accurate network data for such equipment was largely unavailable. Such equipment was included in the network data and the GIC distributions in them were estimated only for the purposes of improving the accuracy of the calculations of GIC distributions in the transmission network belonging to PLQ. The author does not advise that any company other than PLQ base the development of mitigation strategies on the results of this thesis and takes no responsibility for damages incurred by companies that do so.

Chapter 2

Theory

2.1 GIC Calculations given Uniform Geoelectric Fields

To achieve the goals of this project, a method for the calculation of the GIC distribution in a power network given specified uniform geoelectric fields was required. Several decades ago, a theoretical algorithm by which this calculation can be performed for an arbitrary network was presented in [26]. To avoid certain computational issues however, a method different but equivalent to that of [26] was chosen; the method is known as the Nodal Admittance Matrix Method or NAM Method and is discussed in the following Section.

2.1.1 Nodal Admittance Matrix Method

This method is taken from [40]. Its main advantage over that of [26] is that it operates on conductances instead of resistances. The virtual nodes which represent the point between the common and series windings of an autotransformer require infinite grounding resistances due to the fact that they are not connected directly to ground. Implementing the method of [26] in software therefore requires that one approximates these with sufficiently large numbers, while in the NAM Method these infinite resistances are represented exactly by conductances of zero. The NAM Method also has the advantage that its output is an array of node voltages whereas the method of [26] calculates an array of grounding currents. These grounding currents are in fact the GICs flowing through the substation Earth grids when a network of multiple voltage levels is being represented and the transformer winding GICs cannot be easily calculated using these.

In the NAM Method, the circuit to be solved is decomposed into a system of nodes and branches between the nodes. All impedances are inverted and represented by admittances. The problem of calculating the GICs in a power network at a specific point in time is treated as the solution of a DC circuit. Hence when applying the NAM Method the admittances are in fact all conductances. To maintain notation consistent with the literature however they are referred to generally as admittances here. Each node m has an associated admittance to ground y_m as well as an associated branch admittance y_{mn} between itself and each other node n. All branch admittances between nodes which are not connected directly via a branch are zero. All voltage sources in series with the branches of the network are converted to equivalent current sources in shunt with the branch admittance via Ohm's Law. For the general branch between nodes m and n and the voltage V_{GMDmn} induced along the branch by the geomagnetic disturbance, the equivalent source current is given by:

$$j_{mn} = V_{GMDmn} \times y_{mn} \tag{2.1}$$

The total of the source currents from all branches connected directly to each node are then calculated and these are assembled into a column vector $[J]$ with each row corresponding to each node m in the circuit. In general for row m of $[J]$:

$$[J]_m = \sum_{n}^{N} j_{mn} \tag{2.2}$$

Note that N is the total number of nodes; the summation is over all nodes in the circuit. An N by N admittance matrix $[Y]$ is assembled each row and column of which corresponds to a node; in general the element in row m and column n of $[Y]$ refers to node m and node n of the circuit. The off-diagonal elements of $[Y]$ are constructed via:

$$Y_{mn} = -y_{mn} \tag{2.3}$$

Note that y_{mn} is the branch admittance between nodes m and n. The diagonal elements of $[Y]$ are constructed via:

$$[Y]_{mn} = y_m + \sum_{n=1}^{N} y_{mn} \tag{2.4}$$

Note that y_m is the grounding admittance of node m and the summation is over all nodes in the circuit. A column vector containing the solved voltages of each node in the circuit in the same order as $[J]$ is then solved via the following matrix equation:

$$[V] = [Y]^{-1}[J] \tag{2.5}$$

Once Eq. (2.5) has been solved, the currents in all branches in the circuit can readily be calculated using the branch admittances and Ohm's Law.

2.1.2 Application of the NAM Method to the solution of a GIC Distribution in a Power Network

In the application of the NAM Method to the solution of the GIC distribution in a power transmission network, the transmission lines and transformer windings constitute the branches of the circuit and the buses and substation earth grids of the network constitute the nodes. In this thesis buses are referred to as virtual nodes and substation earth grids are referred to as real nodes to distinguish the former which have no direct connections to a remote earth from the latter which do.

All single phase transformer winding resistances and single phase transmission line resistances must be divided by three before being used in GIC calculations. The reason for this is that GICs distribute themselves evenly between all three phases simultaneously. The resistances presented by the three phases must therefore be added in parallel which means effectively that they must be divided by three. The sum of the GICs in each of the three phases flows through the substation Earth grids out towards remote Earth; hence the resistances of the earth grids need not be divided by three. For use in Eq. (2.4), all of these resistances are inverted into conductances, which are referred to generally as network admittances to maintain consistent terminology with the literature.

When applying the NAM Method to the power transformers in a power transmission network, fully-wound transformers and autotransformers must be treated differently since the primary and secondary circuits are connected directly in the case of the latter. For both types of transformers the windings are treated as branches. The LV windings are represented by branches connecting the virtual nodes representing the LV buses to the real nodes representing the earth grids. For fully-wound transformers the HV windings are represented by branches connecting the HV bus nodes to the earth grid nodes, whereas for autotransformers the HV windings are represented by branches connecting the HV bus nodes to the LV bus nodes. Fig. 2.1 depicts the distinction between the modelling of full-wound transformers and auto-transformers in the NAM Method; note that the windings are represented by resistances; in the NAM method they are actually represented with admittances.

The effect of the GMD-induced geoelectric fields is represented by voltage sources

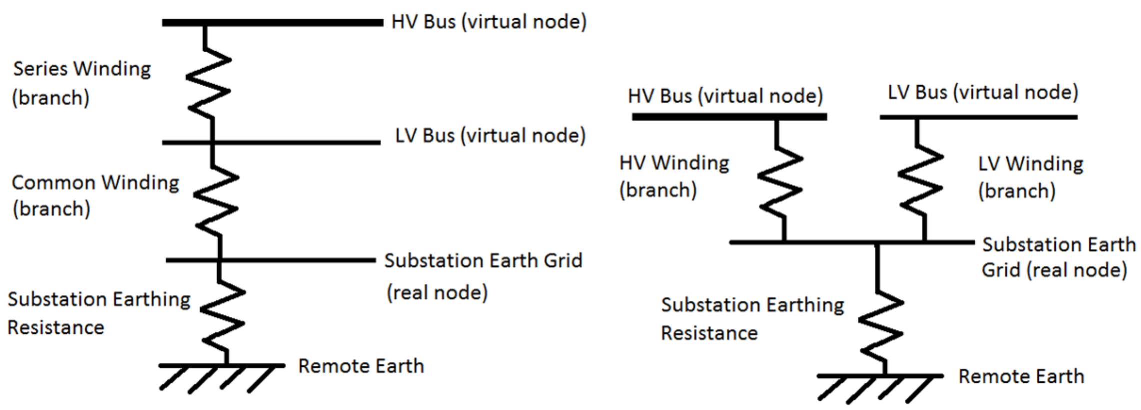

Figure 2.1: Representations of autotransformers (left) and full-wound transformers (right) in the NAM Method

in the transmission lines. To represent non-uniform fields correctly, it is necessary to place the voltage sources in series with the transmission lines and not at the grounding points; the reasoning behind this is explained in [28]. When used in the NAM Method, these are converted to equivalent current sources as described in the previous Section.

2.2 Geoelectric Field Estimation Techniques

In this thesis methods were required by which the geoelectric fields induced during space weather disturbances could be estimated using geomagnetic data recorded at specific locations. Two methods, both of which involve only one-dimensional conductivity models, are described in the following two Sections. The first of these, taken from [33], is referred to generally as the spectral domain method and the second, taken from [38], is referred to generally as the temporal domain method.

2.2.1 Spectral Domain Geoelectric Field Estimation Method

In the work of [33], a seven-layered one-dimensional conductivity model is used to describe the Earth. The atmosphere above the top layer is treated as an infinite half-space with zero conductivity, while the bottom layer of the Earth is also an infinite half-space i.e. it has an infinite extent downwards. As per the usual convention in the field of geomagnetism the z axis denotes depth i.e. $z = 0$ constitutes the surface of the Earth and values of z greater than zero refer to increasing depths within the Earth. The conductivities and layer thicknesses which were considered applicable to the Australian continent and which were used in this thesis were taken from the right-most column of Table 1 in [33]. This conductivity model was scaled from a model by [41] and will henceforth be referred to as the Campbell conductivity model in this thesis.

The primary magnetic field B_x induced by currents external to the Earth is Fourier transformed into the complex frequency domain and denoted $\tilde{B}_x$. A tilde will be used to represent Fourier domain quantities in general. A frequency dependant surface impedance function $\tilde{Z}_N$, the original derivation of which for a generalized one dimensional conductivity model of N-layers is detailed in [39], is then applied to $\tilde{B}_x$ to yield the frequency domain geoelectric field $\tilde{E}_y$:

$$\tilde{Z}_N(\omega) = i\omega\mu_0 \left(\frac{(1 - r_n exp(-2k_n d_n))}{k_n(1 + r_n exp(-2k_n d_n))} \right) \tag{2.6}$$

$$\tilde{E}_y = \tilde{Z}_N \tilde{B}_x \tag{2.7}$$

The spectral domain surface impedance function, an iterative formula which is clearly impractical to solve analytically for seven layers, applies the geoelectromagnetic induction caused by all layers in the conductivity model to the spectral domain magnetic field. Following the application of Eq. (2.7), $\tilde{E}_y$ is inverse-Fourier transformed to yield E_y, the geoelectric field at the surface of the Earth in the time domain. An algorithm such as the Fast Fourier Transform is used to implement the Discrete Fourier Transform and Discrete Inverse Fourier Transform required for the computation.

2.2.2 Temporal Domain Geoelectric Field Estimation Method

Another method for estimating geoelectric fields is to solve temporal domain integral induction equations using numeric techniques. If a one dimensional conductivity model with only one layer is used then the temporal domain convolution integral becomes quite simple. In this thesis the method discussed in [38] was implemented. This model is described below. The temporal integral equation to be solved for a one dimensional one-layered conductivity model, taken from [38] is:

$$E_y(t) = -\frac{1}{\sqrt{\pi\mu_0\sigma}} \int_{-\infty}^{t} \frac{dB_x}{dt'} \frac{1}{\sqrt{t - t'}} dt' \tag{2.8}$$

The directions x and y are perpendicular horizontal directions which are both on the plane to which the vertically incident plane wave representing the geomagnetic disturbance is normal. As per Faraday's Law the induced geoelectric field is always in the direction perpendicular to the changing magnetic field; if x denotes north then y denotes west and if x denotes east y denotes north. Note that t is a constant within the integral of Eq. (2.8) while the variable t is the variable of integration. Note also that the derivative of the horizontal component of the magnetic field is not a partial derivative because the primary magnetic field is assumed to be spatially uniform (at least in x and y) and that this derivative is with respect to t' and not t, i.e. it must be kept inside the integral.

According to [38] this integral equation can be solved numerically using the following formulae (note that $T_{n-1} \leq t \leq T_n$):

$$B(t) = B_{n-1} + \frac{(t - T_{n-1})}{\Delta}(B_n - B_{n-1}) \tag{2.9}$$

$$E(T_n) = \frac{2}{\sqrt{\mu_0 \sigma \Delta}}(R_{N-1} - R_N - \sqrt{M} b_{N-M}) \tag{2.10}$$

$$R_N = \sum_{n=N-M+1}^{N} b_n \sqrt{N - n + 1} \tag{2.11}$$

The meanings of each of the variables are displayed in the following table.

Table 2.1: Meanings of Terms in Eq. (2.9) to Eq. (2.11)

Variable	Meaning
$B(t)$	Instantaneous geomagnetic field intensity.
T_n	Current timestep in the iterative calulcation.
$E(T_n)$	Horizontal geoelectric field intensity calculated at the current time step.
M	Number of previous time steps considered in the calculation.
σ	Vertically homogenous Earth conductivity.
Δ	Time step interval used i.e. $T_n - T_{n-1}$.
μ_0	Permeability of free space (the Earth is assumed to be non-magnetic).

These iterative equations calculate the geoelectric field using the assumptions that the changes in the horizontal geomagnetic field magnitude between each time point can be accurately approximated as linear variations; this is true if the geomagnetic variations of interest are of frequencies sufficiently lower than the Nyquist frequency i.e. half of the sampling frequency.

2.3 A Model for the Geomagnetic Coastal Effect

It became a crucial step later in this thesis to model the influence of the geomagnetic coastal effect on the GIC distribution in the Queensland power transmission network.

In a later Section of [29] equations are developed which describe the geoelectric fields a short distance inland from a generalized coastline during geomagnetic disturbances. The first equation describes the enhanced potential difference between the coastline and a small distance inland due to the component of the geoelectric field which is perpendicular to the coastline. The second equation describes the reduced component of the geoelectric field which is parallel with the coastline. These equations are reproduced below.

$$V_u = \frac{2\mu_0^{1/4} x^{1/2}}{\sigma^{3/4}\pi^{1/2}\Gamma(3/4)} \int_0^t \frac{1}{(t-t')^{1/4}} \frac{\partial H_0(t')}{\partial t'} dt' \tag{2.12}$$

$$E_v = \frac{\mu_0^{3/4} x^{1/2}}{\sigma^{1/4}\Gamma(1/4)} \int_0^t \frac{1}{(t-t')^{3/4}} \frac{\partial H_0(t')}{\partial t'} dt' \tag{2.13}$$

Note that as subscripts, u denotes the direction perpendicular to the coastline and v denotes the direction parallel with the coastline, while the variable V in Eq. (2.12) is a voltage. Note also that x is the distance inland from the coastline in metres.

These equations were developed using the Wiener Hopf technique and with the assumption that the ocean can be modelled as an infinitely thin, infinitely conductive sheet; a common assumption in geoelectromagnetic induction theory. It should also be noted that they are only deemed to be valid for short distances inland in [29].

2.4 Effective Transformer GIC

The extent to which given levels and directions of HV and LV winding GICs will cause a transformer to saturate depends on the number of turns of each winding, as well as the type of transformer considered. If the GICs in one winding flow in the opposite direction to those in the other winding then the magnetic flux produced by each will be in opposition and less severe saturation of the core will occur. A useful quantity to which the saturation of the core can be related directly is therefore required to conduct GIC studies on power networks. This quantity is referred to as the effective GIC flowing through each transformer. For a full-wound transformer with a turns ratio N and HV and LV winding GICs (with the same polarity convention) of I_H and I_L respectively the formula for calculating the effective GIC, taken from [52], is:

$$I_{eff} = \left| \frac{(NI_H + I_L)}{N} \right| \tag{2.14}$$

Note that the effective GIC is always positive; the same amount of saturation for a given transformer core type will occur regardless of the direction of the term inside the absolute magnitude operator in Eq. (2.14). For an autotransformer with a turns ratio N_A and series and common winding GICs of I_S and I_C respectively the formula for the effective GIC, again taken from [52], is:

$$I_{eff} = \left| \frac{(N_A I_S + I_C)}{(N_A + 1)} \right| \tag{2.15}$$

Note that the turns ratio of an autotransformer is not the same as the ratio of the voltages of the HV and LV buses to which it is bonded. The relationship between the turns ratio of an autotransformer and the HV and LV bus voltages V_H and V_L is shown in Eq. (2.16):

$$N_A = \frac{V_H}{V_L} - 1 \tag{2.16}$$

The effective GIC flowing through a power transformer can be used to compare the severity of the GICs flowing through several transformers of different turns ratios and designs.

Chapter 3

Space Weather and Power Networks

For many decades now, it has been understood that geomagnetic storms can cause problems for power transmission networks on Earth [1]. The term geomagnetic storm encompasses a vast range of field and plasma disturbance events in the terrestrial magnetic field and the near-Earth space environment. The disturbances on the surface of the sun which cause these events are referred to generally as solar storms and involve ejections of plasma more intense than those normally present in the solar wind; the largest of these are referred to as Coronal Mass Ejections or CMEs. When these clouds of plasma are directed towards the Earth they interact with the magnetic field of the planet, the magnetosphere, upon arrival. The electromagnetic and plasma interactions between the magnetosphere and the solar wind and all disturbances which precipitate from these are referred to generally as space weather.

The final result as far as power utilities are concerned is the entrance of unwanted currents, which are known as Geomagnetically Induced Currents or GICs, into their power networks through wye-grounded transformers and grounded reactors. These low frequency currents, typically of frequencies in the milli-Hertz range [2], cause half-cycle saturation of power transformers [3], which in turn can cause both increased reactive power consumption of the transformer and internal heating of the device itself. Depending on the loading of the power system during the event, the former can lead to voltage collapse of the system as occurred in the Hydro-Quebec system in March of 1989 [4] and the latter can damage the power transformer enough that it needs to be replaced [5]. Transformer cores also inject harmonic currents into the power system under these conditions which can cause relays to trip unnecessarily [6].

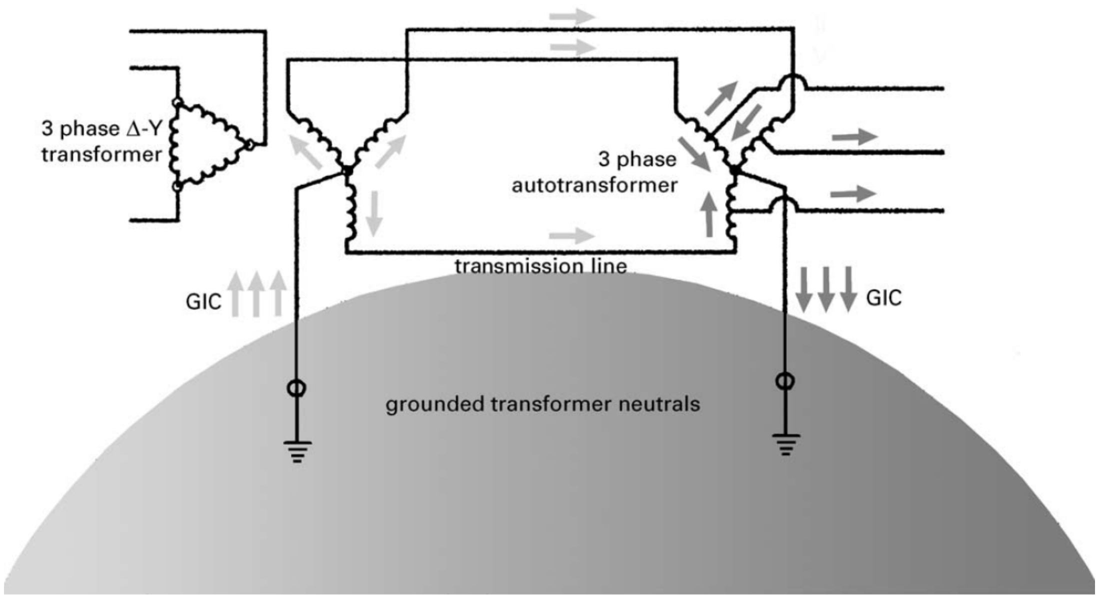

Figure 3.1: GICs entering a power transmission network [7]

Geomagnetic storms are characterised by periods of decreased strength of the northward or H component of the geomagnetic field lasting typically for a few days and interspersed with other disturbances of a wide range of frequencies [35]. It should be noted that the eastward component of the terrestrial geomagnetic field is usually referred to as the D component and the component which points into the Earth is usually referred to as the Z component. Geomagnetic substorms, which occur intermittently throughout storms, are further excursions of the field with periods ranging from ten minutes to two hours. Variations in the geomagnetic field in general induce geoelectric fields across the surface of the Earth over large distances. These geoelectric fields drive GICs through power transmission lines via their grounding points, which due to their low frequencies are generally treated as quasi-DC currents. If the geoelectric fields induced are severe enough they can cause voltage stability problems across entire power transmission networks because they affect large areas of land simultaneously.

In [1] and references therein the forecasting and general study of GICs in a power network is separated into two steps requiring expertise from different fields. The first step is to calculate the geoelectric field at the Earths surface in the absence of the power network. In general, this requires measurements of solar disturbances, the solar wind and the magnetosphere via satellites as well as geomagnetic field measurements via ground based geomagnetic observatories. For the purposes of geomagnetic storm forecasting, this data must be interpreted using physical models of the magnetic field variations and plasma dynamics of the Inter-planetary Magnetic

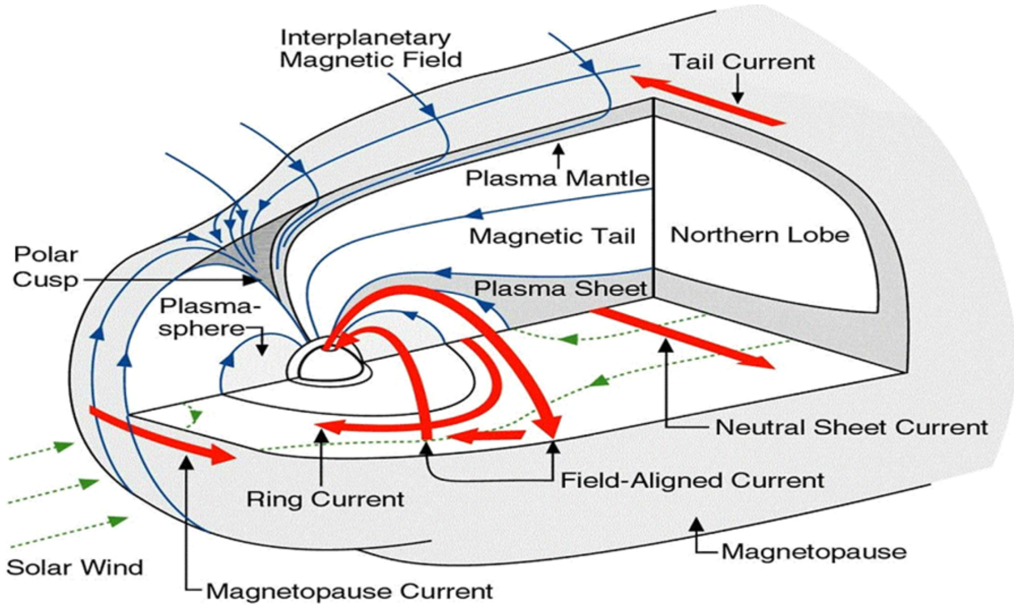

Figure 3.2: The Magnetosphere and Magnetospheric Current Systems

Field (IMF), the magnetosphere and the ionosphere which occur during these storms. The second step, referred to as the engineering step, is the calculation of the GICs which will be present in the network once the geoelectric field in the absence of that network is known and the impact that those GICs will have on the stability of the network. This calculation is based on the topology and parameters of the power network, the saturation characteristics of all power transformers in the network and level of loading at the time of the event [3]. The complexity of both calculations makes it difficult for power utilities to plan for space weather disturbances in general.

For many decades the only countries whose power utilities have been largely concerned with the effects of geomagnetic disturbances on their networks are those at far northern or southern latitudes [2]. This is because auroral electrojets were the only ionospheric current systems understood to drive large GICs, and these expand from the auroral zones which surround the geomagnetic poles of the planet. The auroral electrojets are sheets of current which have total volume-integrated magnitudes on the order of mega-amperes and which flow in the lower regions of the ionosphere at altitudes of roughly 100km. Their enhancement during these disturbances occurs due to sudden increased particle precipitation into the auroral zones via the field aligned currents, otherwise known as Birkeland currents. Such abrupt increases in the Birkeland currents occur during substorms due to sudden and violent reconnection of magnetospheric field lines which have briefly merged with the IMF at the front of the magnetosphere and been dragged to the tail lobes. Magnetic tension builds up in the tail lobes when the rate of magnetic reconnection there is not in equilibrium with that at the front. Magnetic reconnection is the transferral of magnetic potential energy into particle energy (i.e. thermal energy) at the boundaries between magnetic fields of different orientations in regions of space populated with plasma. For a good general explanation of space and plasma physics, refer to [8] or a similar textbook.

In addition to the auroral electrojets, other magnetospheric/ionospheric currents of interest are equatorial electrojets and the equatorial ring current. Both constitute volume-integrated currents on the order of millions of amperes. However, neither of them produces terrestrial geomagnetic field variations as large as those produced by the auroral electrojets in general. Equatorial electrojets are enhancements of the so called solar quiet current vortices where they meet in the equatorial ionosphere due to the near vertically-incident solar radiation and horizontal geometry of the magnetosphere there. These factors combine to create a self-amplifying system of Hall and Pedersen currents. The presence of solar UV and EUV radiation causes the increased conductivity in this region of the ionosphere and this largely facilitates the presence of these electrojets. This is regulated by the rotation of the planet in general and does not cause changes in these current jets as rapid as the expansion of the auroral electrojets during geomagnetic storms. The ring current is a circulation of particles in the Van Allen radiation belts which are situated at altitudes of several Earth radii and hence produce comparably small geomagnetic variations as well. For a good review of magnetospheric and ionospheric current systems during geomagnetic storms, see [9]. For a review of the effects which geomagnetic storms have on the winds, chemical composition and structure of the ionosphere and the thermosphere, see [10] and [11].

Recently events known as Sudden Impulses (SIs) or Sudden Commencements (SCs), which have been observed via geomagnetic measurements for decades, have been linked with GICs of significant magnitudes in mid and low-latitude regions of the planet [12], [13]. The geomagnetic signature of an SC is an abrupt increase in the horizontal geomagnetic field: [14] defines it as a rapid change in the H component of the geomagnetic field of at least 5nT over ten minutes preceded by a period which was geomagnetically quiet.

In [12] several cases of GICs driven by SC-induced geoelectric fields are described. The GICs measured in central Japan are particularly interesting as these occurred at stations of mid to low-latitude positions. This study discusses the use of Earth models with multiple layers of differing conductivities for calculating geoelectric fields induced by known geomagnetic variations. It reveals that the geoelectric field calculated can differ by multiple orders of magnitude depending on the conductivity model used. It is also discussed that the SC which occurred on the 24th of March

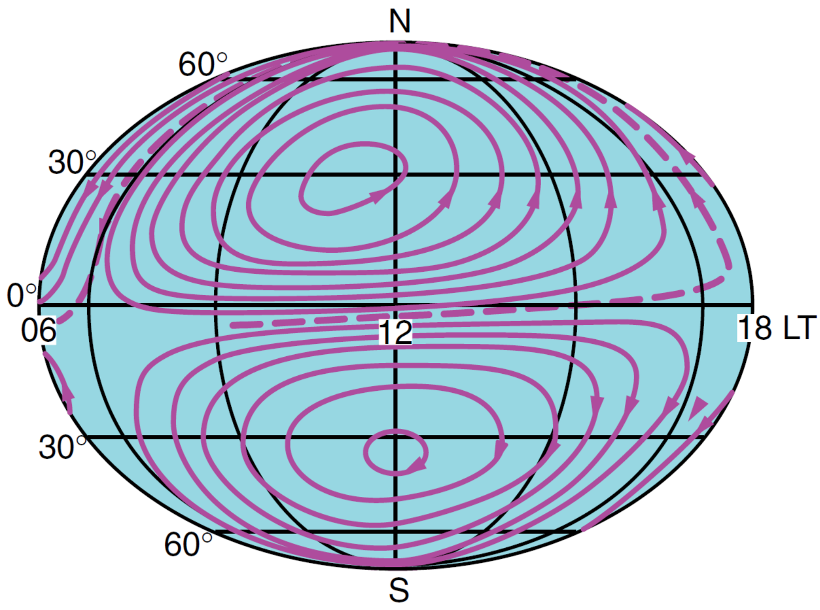

Figure 3.3: Dayside view of the Solar quiet (Sq) ionospheric current vortices which form the equatorial electrojets where they meet at the equator [9]

in 1991 generated sizeable geoelectric fields on both the day and night sides of the planet as indicated by measurements in geomagnetic observatories in Japan and the United States. This indicates that risks posed to power grids by SC driven GICs do not necessarily vary with the time of day. In [16] it is indicated that SCs produce geoelectric fields of coherent direction across entire continents. The same SC as discussed in [12] is said to have caused a GIC of 175 amperes which is one of the largest ever recorded in the Finnish power network. The geomagnetic variations across Western Europe for the SC studied in this article indicate a northward geoelectric field over Finland gradually curving into an eastward geoelectric field over the United Kingdom and further south of this.

An SC begins with the arrival of a discontinuity of the solar wind dynamic pressure at the magnetopause. The physical model for an SC understood to be accurate by the author is that of [36]. In this model, the total disturbance field of the SC as measured on Earth is broken into two fields; the DL field and the DP field. The DL field is characterized by a step function-like increase of the H component. The DP field is characterized by a two pulse structure i.e. a peak and a trough in the strength of the H and/or the D component, the order of which depends on the Magnetic Local Time (MLT) at which the disturbance is observed.

The DL field is caused by the dusk to dawn polarisation current which propagates through the magnetosphere as a magneto-hydrodynamic (MHD) fast mode wave. This current, which closes with the enhanced magnetopause current, facilitates the compression of the magnetospheric plasma and ends shortly after the magnetopause current has increased to a value high enough to generate a force which balances the increased dynamic pressure of the solar wind. The DL field is dominant at lower latitudes. The Alfven velocity of the magnetospheric plasma and the time it takes for magnetospheric convection to adjust to the new compressed state of the field are both important factors in determining the duration of the SC. The magnitude of the solar wind pressure discontinuity also affects both the total amplitude and duration of the SC. The possible durations of SCs is important information for power utilities as both the large scale stability of a power system and the thermal stability of an individual power transformer are likely to exhibit some criticality with respect to the amount of time for which they are exposed to a given level of GICs.

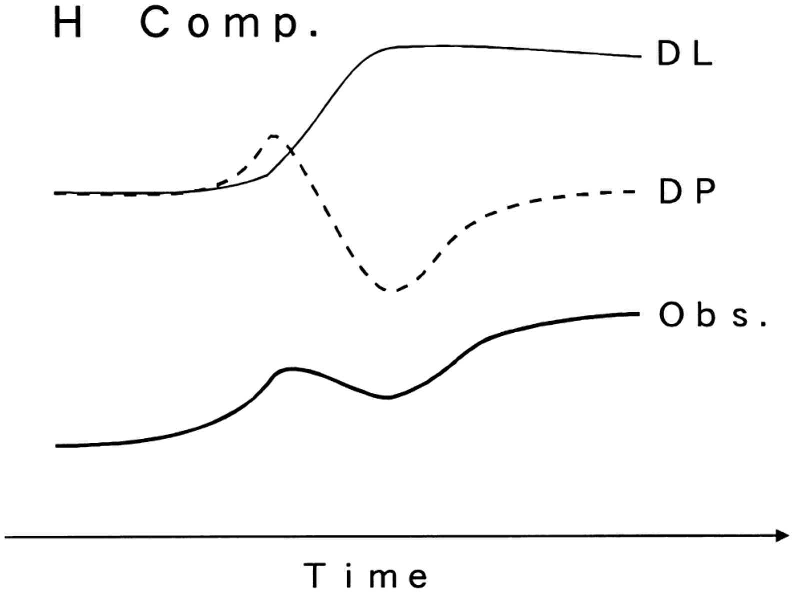

Figure 3.4: Decomposition of the SC disturbance field into the DL- and DP-subfields [50]

The polarization current also excites another mode of MHD wave; the Alfven mode. Unlike the fast mode which is part compressional, the Alfven mode only involves oscillations of ions and the magnetic field which are transverse to the direction of propagation, which is always the direction of the field lines [8]. These Alfven waves energize gyrating radiation belt particles sufficiently to cause them to spiral down into the polar ionosphere; this constitutes the field aligned currents. These particles increase the conductivities of the auroral ionosphere and in turn drive a twin-vortex current system. It is these ionospheric current systems which generate the DP disturbance. The DP field has a two pulse structure because the FACs, and therefore the twin ionospheric vortex currents, reverse polarity after tailward passage (and partial reflection) of the polarisation current.

The variations in average intensity of the DL field and the DP field with latitude result from the differing spatial distributions of the current systems driving them. The DP field dominates at high latitudes and has decreasing amplitude with decreasing latitude then suddenly reappears, on the dayside only, at equatorial latitudes. The DL field has the greatest magnitude at the equator and gradually decreases with increasing latitude. Initial consultation of power industry literature may lead one to believe that SC events generally occur with equal intensity and polarisation all around the planet. This would imply that they tend to generate geoelectric fields which are fairly uniform and that it might therefore be permissible to simulate the GIC distributions driven by them using uniform geoelectric fields. Consultation of the geophysical literature however reveals that the magnitudes and waveforms of the disturbance fields caused during SCs vary significantly with Magnetic Local Time (MLT) and Magnetic Latitude [37].

Apart from the connection between GICs and SCs, there are two other reasons that power utilities in all countries around the world should re-evaluate their systems vulnerability to space weather. Firstly, larger GICs develop in transmission lines of lower resistance which stretch over longer distances. Lines which operate at higher voltages are built with thicker conductors and these present lower resistances per unit length to GICs, enhancing their development for a given geomagnetic disturbance. So as power networks around the world are expanded with longer transmission lines operated at higher voltages, their vulnerability to GICs increases [5]. Secondly, the most severe geomagnetic storm which can occur is not known and difficult to predict. The largest geomagnetic storm which was ever recorded occurred in 1859, before any power transmission networks existed [18]. It recorded 400nT on the aa index which is a measure of the overall planetary disturbance to the magnetosphere caused by a geomagnetic storm.

In a recently published article the risk posed by space weather to Australia was evaluated using statistical studies [17]. A comprehensive review of GICs produced at different latitudes around the world during geomagnetic storms was conducted in this article. Using the GIC index developed therein, which is based on geomagnetic observatory data, it was assessed that Queensland reached at most the low risk level during all geomagnetic disturbances over the last two solar cycles. A more comprehensive study of space weather risk for each power utility in Australia is however still necessary.

In [30], magneto-telluric techniques were used to derive a 10-layered conductivity model for the Grassridge substation in South Africa. This conductivity model was then used to determine network coefficients for the prediction of GICs there as derived in [31]. These parameters are determined empirically using historical geomagnetic data and GIC measurements and summarise the network topology and other factors which determine the GIC generated at a particular point in a network for a given geoelectric field. This method saves time and is often more feasible than a physical GIC model for the system. This paper also presents iterative formulae for approximating the geoelectric field induced at the surface of an Earth of uniform conductivity by approximating all variations in the geomagnetic field between measurements as linear; this formula was originally presented in [38]. A method to calculate the distribution of GICs in a network of grounded conductors given a known, time invariant geoelectric field is developed in [26]. The method requires the gathering of network topology and DC resistance information into a system of matrices and then uses Ohm's Law and Kirchhoffs voltage law to solve the corresponding matrix equations for the transformer neutral GICs. Physically-derived techniques for calculating the distribution of GICs across an entire power transmission network given the geoelectric field driving them such as this one should be adopted by all power utilities in the long term.

In [27] the techniques derived in [26] are used to calculate the currents in a simple V-shaped transmission system with five wye-grounded transformers and transmission lines with two orientations. The effects which the orientation of transmission lines with respect to a uniform geoelectric field can have on the GICs in a power system are demonstrated. It also demonstrated that installing a series capacitor in arbitrary positions in the network, though they block the flow of GICs because they present an open circuit to a DC current, can actually increase GICs at individual neutrals and even the total GIC at all sites. For series capacitors to solve GIC problems in any complex power system they would have to be installed in series with every transmission line connected to a wye-grounded transmission line; an economically infeasible option for any utility.

Several important points about the geoelectric fields which drive GICs are demonstrated in [28]. Realistic geoelectric fields are not uniform; in general they exhibit spatial variations in magnitude and direction and drop off to zero at infinity. This means that they are non-conservative fields; this fact has two consequences for GIC calculations. First of all, to calculate the voltages necessary to model GICs in a power network, one must integrate the geoelectric field along the Earth directly below the transmission line. Secondly, the voltage sources which apply these voltages to the network must be modelled in series with the transmission lines themselves and not at the grounding points of the network. The modelling technique of [26] accounts for both of these.

To assess risks posed by space weather, the nature of power transformer saturation when subjected to GICs must be understood. In [3] the author gives a good physical explanation of the half cycle saturation of a power transformer core while under the influence of GIC. In [19] a 400kV power transformer with a 3 phase, five limb core is used for experimental GIC-saturation tests. It is found that the once the transformer is saturated, the apparent, real and reactive power consumption of the machine increases linearly with GIC. This is also supported by [20]. This paper claims that as a result of the tests performed, it can be concluded that the most critical temperature rise under full loading conditions for this transformer could be 170-180C and that this is acceptable under IEC standards, dismissing the hazard posed by GICs to power transformers. The drawing of this conclusion however is likely to have been influenced by the fact that power transformers in the Finnish power grid are generally not operated very near to their ratings, as indicated in [21] to be the reason that even the largest GICs ever measured in the Finnish power transmission network have never caused any significant problems.

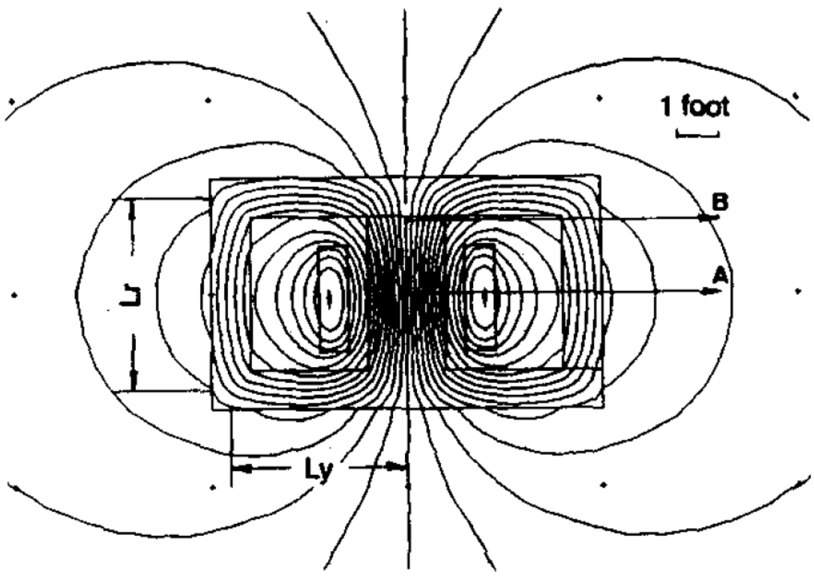

Figure 3.5: Magnetic flux distribution of a single phase transformer core in half-cycle saturation [25]

In [22], the authors perform tests on small scale models of power transformers with magnetic and non-magnetic materials as well as models of normal scales in order to study their characteristics under DC saturation. This study predicts low risk of physical damage to the transformer given the heating they measured in an ideal laboratory environment while the transformer was not loaded: this is also true of [19]. These studies do not consider the possibility that the operation of transformers at temperatures which are even slightly excessive could cause partial degradation to the paper insulation of the transformer windings and contribute significantly to their eventual failure. This is of particular concern for older power transformers which are operated close to their power ratings. The author gives a good review of diagnostic techniques which are used to assess the condition of insulation on old transformers in [23]. In [24] findings of the Dissolved Gas Analysis (DGA) studies of several power transformers in South Africa are detailed; these findings reveal that the eventual failures of these machines were all linked to a geomagnetic storm in November of 2003. This provides evidence that GICs can damage power transformers significantly, even if the transformer does not break down immediately during the storm.

Power transformers with different core constructions present magnetic paths of differing reluctance to the zero sequence magnetic flux forced through them when GICs flow into the neutral [25]. Because of this, some core constructions will result in more severe half-cycle saturation for a given GIC value than others. In [7] the general order of GIC vulnerability by core type from most vulnerable to least vulnerable is:

1. Single phase core
2. Three phase conventional type (or shell type) seven leg core
3. Three phase conventional type core
4. Three phase core form five leg core
5. Three phase core form three leg core

The single phase core type saturates most readily because it presents a very low reluctance path to zero sequence magnetic flux which means that the field strength inside the core material becomes very high and extremely large excursions of the magnetizing current occur. To assess the vulnerability of their grid to space weather, an obvious step for every power utility is to review the core types of their power transformers.

An important aspect of the risk posed to power networks by space weather which is difficult to model is the geomagnetic coastal effect. This phenomenon of geomagnetism is well defined in [35]. In the presence of stark lateral conductivity variations, such as those presented by a coastline, the geoelectric fields induced during geomagnetic disturbances are significantly altered from what they would otherwise be. The excitation of eddy currents in the highly conductive seawater and the conductive regions of the Earth below ocean floors complicate the inductive response to such disturbances [39]. In [29] it is demonstrated that the expected effect in close proximity to a coastline is enhancement of the component of the horizontal geoelectric field perpendicular to the coastline and reduction of the component parallel to it. The simplicity of this result can of course be expected to break if the coastline varies significantly in direction over sufficiently large length scales. The problem of the alterations to geoelectric fields induced during space weather disturbances in close proximity to coastlines is an important one for GIC forecasting in general.

As space weather physics is a natural science it progresses forward predominantly with careful, scrupulously checked and copiously databased long term observation and the verification and refinement of theoretical models via analysis of and comparison with these observations. The theoretical models tend to be more empirical than derived directly from fundamental physical laws for the simple reason that the systems studied are far too large and complex to allow for the latter. Although outstanding theoretical foresight occasionally predicts future observations, such as the prediction of the existence of the magnetosphere by Chapman and Ferraro in the 1930s before any extra-terrestrial measurements of the field had been made, the models tend to trail observations by some considerable distance. One cannot therefore assume that the upper bound on all possible geoelectric fields which could be induced in any region of the world can be known with any certainty, whether such upper bounds were predicted with the current models or are based on the trends of historical data.

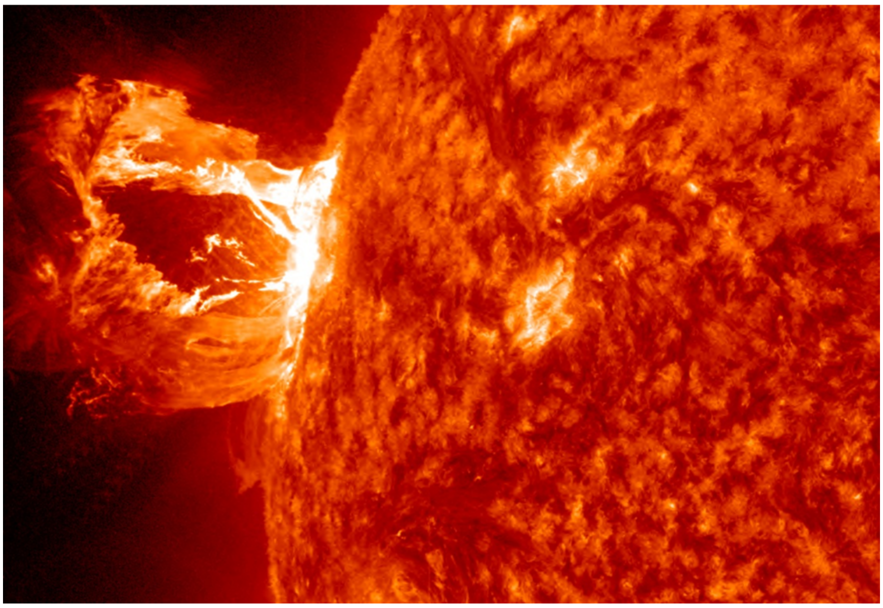

Figure 3.6: The surface of the sun; oftentimes less than peaceful, it conceals a realm of scarcely understood physical processes [51]

When one notes that longer transmission lines of higher voltages couple with space weather disturbances more effectively, it becomes clear that the total period of human observation of that coupling process for transmission systems of modern lengths and operating voltages is far less than one hundred years. The strongest recorded geomagnetic storm occurred over 150 years ago. Geomagnetic polarity reversals are separated by periods of hundreds of thousands to millions of years. During these events several moments higher than the dipole moment appear chaotically in the Earths magnetic field, thereby entirely changing the nature and possible severity of geomagnetic storms. The inner dynamics of the sun could conceal processes which modulate the severity of plasma ejection events on time scales longer than the total period of human observation as well.

It would obviously be impractical to spend excessive money modifying all power infrastructures so as to make them impervious to space weather. Instead it must be recognised that there is a possibility that events which modern power transmission networks are not designed to cope with could occur in the future. But if the engineering community makes an effort to better understand space weather physics and geomagnetism so as to facilitate more efficient communication between the power industry and the researchers in these fields then perhaps faster and more effective mitigation strategies could be developed.

Chapter 4

Development of Methods for GIC Estimation

In order that GIC distributions in the Queensland network could be calculated, data describing this network need to be collected and software had to be written to perform the calculations. Both of these are described in this Chapter.

4.1 Network Parameters

Several types of data are required to calculate GIC distributions in power networks. These datasets for the Queensland network are herein collectively referred to as the network data. The network data was stored in an Excel spreadsheet as it was collected. The types of data which were collected, the difficulties which were encountered and the approximations which were made while gathering them are discussed in the following Sections.

4.1.1 Network Topology and Transmission Line Resistances

All data pertaining to the topology of the network was extracted from a PSS/E fault study casefile. These data included the eight-character names of all buses in the network, the lengths and resistances of all transmission lines in the network and the buses to which they were connected at either end. In the PSS/E files used by PLQ impedances, including resistances and reactances of transmission lines, are stored as per-unit quantities on a 100MVA base. Therefore in order to attain the per-phase resistances of each transmission line all feeder or branch resistances taken from the casefile were multiplied by an impedance base calculated using the operating voltage

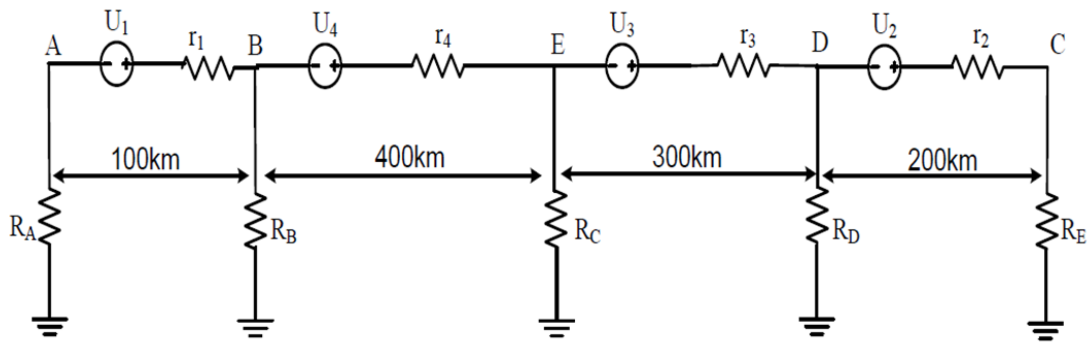

Figure 4.1: All of transmission line resistances, transformer winding resistances and substation earth grid resistances are required for the calculation of a GIC distribution in a power network [52]

of the branch and a 100MVA power base.

In principle, the DC resistances of all equipment should be used to calculate GICs in a power network. The DC resistance of a conductor differs to its AC resistance due to the skin effect. The time-varying nature of the alternating current induces a time-varying magnetic field which in turn causes a secondary induced electric field; this secondary electric field opposes the original field, most significantly in the centre of the conductor and the result is diminished current density. The resistances used in power system analysis are the slightly higher resistances experienced by AC currents at the nominal frequency. It was found however that the ratio of AC resistance to DC resistance for the majority of conductor types in the network range from about 1.001 to 1.02, while a small number are as high as 1.2. Since the task of identifying the conductor type of each feeder in the network would have been highly time-consuming and resistance errors of 0.1% to 2% are insignificant in comparison to other inaccuracies in the study, the AC resistances were considered sufficient for this project.

4.1.2 Transformer Data

4.1.2.1 Transformer Winding Resistances

Although they are generally smaller than the total resistances of the transmission lines, the transformer winding resistances still influence the calculation of GICs in a power network significantly. It was decided that rather than trying to calculate the winding resistances of the transformers in the network using the complex positive sequence impedances in the PSS/E casefile, they should instead be taken, where possible, from the original test reports for each transformer. This way it could be known for certain that no approximations in the values of these resistances had been made, other than those made knowingly by the author. The presentation format of test reports for power transformers varies significantly between manufacturers; however the vast majority of them contain pages detailing the measurements of the resistances of each winding.

Such data is generally presented in separate tables for each winding with columns for each phase. All power transformers are designed with the impedances in each phase as close as possible to equal so that the three phase currents and voltages passing through them remain balanced. The average resistances between phases were therefore recorded. The temperatures of the oil during winding resistance tests are presented in the test reports. These were recorded and used to scale up the winding resistances to a consistent standard of 75 degrees Celsius. While the operating temperature of each transformer can in practice be significantly higher than this, especially when under excitation by GICs, a consistent standard had to be chosen and 75 degrees was considered a good lower bound on transformer operating temperatures. The rescaling was done via the assumption that the resistivities of the windings vary linearly with temperature in degrees Kelvin which is a good approximation for most metals in the range of normal operating temperatures.

In each test report several rows of resistances of one of the windings, depending on which winding the taps have been built onto, are presented for each tap setting. For each transformer the nominal tap setting was identified and the winding resistance corresponding to this setting was recorded. While in service the tap which is in use varies constantly to balance bus voltages and load flows, however the corresponding variations in effective winding resistances will not be significant. In many reports the winding resistances are presented as values from the HV or LV bushing of one phase to that of another. The resistances required were those of each individual (single phase) winding; hence in such situations for full-wound transformers this value was divided by two. For auto transformers where the winding resistances were presented as values measured from one of the HV bushings to another, this value had to be divided by two and then the resistance of the common winding subtracted from it in order to obtain the series winding resistance. A diagram showing the unique winding orientation of an autotransformer was shown earlier in this report; see Fig. 2.1 in Chapter 2.

In general the following data was recorded; for full-wound transformers the average single phase resistance of both the primary and secondary windings and for auto transformers the average single phase resistance of both the series and common windings. As the transformer winding resistances were recorded manually from hard copy documents the possibility exists that some resistances were incorrectly recorded as a result of human error. The test reports were consulted a second time to check for such mistakes, a few of which were identified and remedied, although in principle there could still be errors in the recordings. The care which was taken in recording this data however is considered sufficient that the results of this study will be reliable in general.

For many transformers on the edge of the network, particularly those belonging to distribution companies, test reports were simply not available. All such transformers were assigned the average winding resistances for their type, depending on whether they were full-wound transformers or auto transformers respectively. The transformer winding resistances were found to lie predominantly in the range of 0.1-2.0 ohms per phase. The resistances of the transmission lines often dominate such values. Accuracy of winding resistances was therefore only deemed to be necessary for transformers which were of critical importance in the Queensland network; accurate winding resistances were recorded for the vast majority of PLQ-owned transformers.

4.1.2.2 Transformer Winding Types

GICs can only enter a power network through transformers with a grounded neutral; all transformers with delta windings therefore inhibit the flow of GICs. Although the primary and secondary windings of the majority of PLQ transformers are wye windings with neutrals bonded to the substation earth grid, a small number of transformers in the network were observed to have delta windings. All network diagrams were carefully checked several times and all such transformers were recorded. Each of these transformers was manually excluded from the study, except for those with wye primary windings and delta secondary windings; all of these which were found were connected to LV buses of operating voltages below 110kV. Such buses themselves were excluded from the study, the reasoning for which is discussed in Subsection 4.1.6.

4.1.3 Shunt Reactor Winding Resistances

Several of the feeders in the Queensland transmission network have shunt reactors at their ends to provide reactive power compensation. These reactors have grounding points in their neutrals and so present paths to GICs and had to be incorporated into the model as well. Although they often have winding resistances an order of magnitude higher than those of power transformers, their effect on the GIC distribution cannot be said to be negligible. The winding resistances and HV buses of all shunt reactors in the network were recorded in the Excel spreadsheet. They were modelled as if they were autotransformers with HV and LV winding resistances each of which were half of the actual winding resistance of the reactor.

4.1.4 Substation Earth Grid Resistances

The resistance from the transformer neutral to a remote earth is the final resistance required in the GIC calculation. These were assumed to be near enough to equal to the Earth grid resistances obtained by direct measurement to test their performance. In principle these two resistances are not equal since the frequency of the injected current, less than 1Hz for GICs and 50Hz for power system faults, are not the same and hence the conductivity of the earth through which the current is dispersed is different. Also, the proximity of one substation to another may mean that the GICs entering each substation change the potentials of the earthing points at the other. Despite these limitations the earth grid resistance measurements were assumed to be applicable to GIC distribution studies as they are in [26].

The grounding resistance measurements of all PLQ substations were recorded as part of the network data. For those substations belonging to distribution companies or generation companies, the average value of all substation grounding resistances was used. As in the case of the transformer winding resistances, the width of the distribution of substation grounding resistances was considered small enough that use of the mean value for substations where no data was available would produce accurate results.

4.1.5 Spatial Data

Of all the data pertaining to PLQ's network which was gathered in this project, that which had to be gathered with the most care was the coordinates of each substation included in the study. Errors in a single degree of latitude or longitude could have meant that transmission line lengths were calculated incorrectly to the order of hundreds of kilometres, which would have translated to significant errors in GIC estimations. All latitude and longitude data collected were of the WGS84 geodetic standard and the decimal degrees format.

Throughout the transmission network there are structures known as tees; locations where three feeders join together on a tower instead of at a substation. The PSS/E casefile also contained fictitious buses corresponding to these tees. The spatial data for the tees in the network were not readily available and had to be sought manually.

Also an issue were the locations of some of the distribution network substations; in general only the locations of the majority of the PLQ substations were known beforehand. The locations of both the distribution substations and the transmission line tees had to be sought individually. Unknown spatial data was found using a spatial database maintained by PLQ.

So that the paths of the transmission lines could be integrated with non-uniform geoelectric fields, data pertaining to the lengths and angles of all subsections of each transmission line were required later in the project. This data was acquired with the help of a Spatial Data Team within PLQ. The issues which were encountered while analysing this data will be discussed later in this thesis. In order to approximate the effects of the geomagnetic coast effect, the shortest distances of each transmission line span in the network from the coastline was required. To achieve this, the coordinates for a series of points along the coastline of Queensland and New South Wales were collected. This data and its application are discussed further in Section 4.5 of this Chapter.

4.1.6 Disassociating the Transmission System from the Distribution Systems

Compared to power transmission networks, power distribution networks generally experience GICs of smaller magnitude during any given space weather event. The reasons for this are that they tend to consist of transmission lines of higher resistances and shorter lengths, both of which reduce their coupling with space weather disturbances. It is therefore reasonable to neglect them when studying distributions of GICs in transmission networks; this was desirable in this project as the distribution networks constitute meshed and complex systems of electrical parameters and spatial data when compared to the transmission system. Also, they belong to other companies and requesting information from them would have been potentially difficult and time consuming.

The process of neglecting the distribution networks involved some important decisions on the approximations which would be made. So that the accuracy of the model was consistent across the network, a minimum operating voltage of transmission lines and buses in the real system to include in the study had to be chosen. A value of 110kV (line to line) was chosen since this is generally the lowest voltage of transmission lines which PLQ owns, although some lines of 110 or 132 kV are owned by distribution companies. All transformers in the network known to be bonded to buses of 110kV or above were included in the network data collected.

4.1.7 Representing the effect of the connections to the NSW Network

The Queensland power transmission network shares connections with the New South Wales power transmission network. Because data for the NSW network could not be readily attained the effect of this network on the GIC distribution in the Queensland network had to be approximated in some way.

The effect which one power transmission network has on the GIC distribution of another when the former is viewed as being external to the latter is to reduce the effective resistance to ground of the final substation of the first system. This is due to the fact that the external power transmission network contains many separate paths to remote Earth when it is viewed as a DC circuit, as is appropriate when studying GIC-flows, hence its Thevenin equivalent resistance is significantly less than the effective earthing resistance of the transformers and earth grid of the last substation in the first system. It is therefore a reasonably accurate approximation to set to zero the effective earthing resistances of substations which are connected directly to other power transmission networks for which data cannot be acquired.

The winding admittances of the transformers at the substations at the edge of the Queensland network which are connected to the New South Wales network were set to 10^{12} Siemens to approximate infinite admittances. The admittances of their Earth grids were also set to this value. Although this approximation had the desired effect of enhancing the GICs in the transmission lines connected to these seubstations and therefore the GICs in the windings of the transformers at substations in close proximity to them, this also meant that the GICs calculated in the windings of the transformers at these substations were unnaturally high. Functionality was written into the MATLAB code to force these GICs to zero after all other calculations had been performed, so that they would not skew the results.

4.2 Code for GIC Calculations given Uniform Fields

As previously mentioned it was necessary in this thesis to have software which could calculate distributions of GICs in power networks given uniform geoelectric fields. Until very recently no commercial software tools were available for this task. Due to the interest in space weather in the power industry over the past few years of this solar cycle, commercial GIC tools are now being developed for PowerWorld Simulator, PSS/E and others. The North American Electric Reliability Corporation have also released open source code to calculate GIC distributions in a power network, however this was learned too late in the project for it to be utilised.

The primary software platform chosen to implement calculations in this project was MATLAB due to its efficient handling of large arrays and matrices of data. A MATLAB function was written to implement the NAM Method given network data loaded from the Excel spreadsheet and a predetermined uniform geoelectric field. This function was called runGICuniform. For the reasons previously mentioned the transmission line resistances and transformer winding resistances were all divided by three in the spreadsheet before being inverted into admittances and then loaded into MATLAB sessions.

Several pieces of MATLAB code were written during this project. As they are discussed repeatedly throughout this document a functional hierarchy of the most important mfiles is shown in Fig. 4.2.

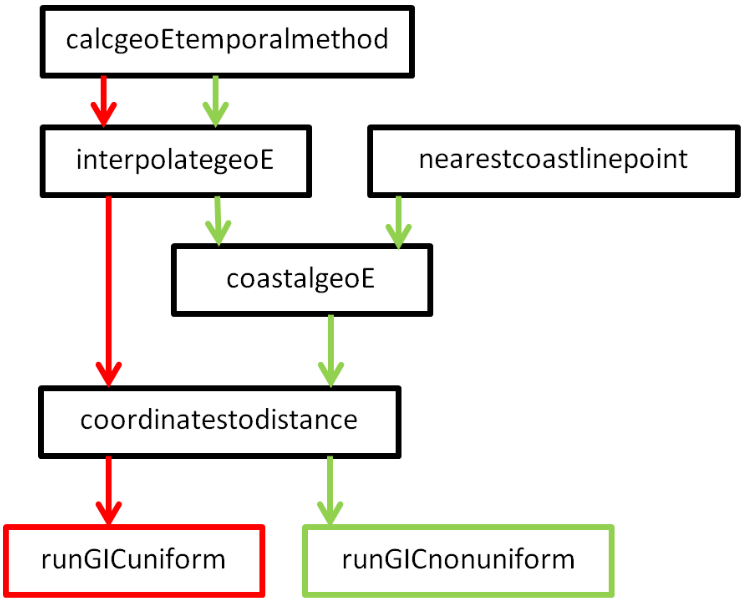

Figure 4.2: Functional hierarchy of code

Several difficulties unrelated to implementation of the NAM Method were encountered when writing runGICuniform. These are discussed in the following two Sections.

4.2.1 Calculating Transformer GICs in the Presence of Neglected Buses

As previously mentioned all buses in the network of operating voltages below 110kV were neglected from the study. In effect this was done by not including such buses in the data which was entered into the Excel spreadsheet. It was therefore necessary to make some careful considerations when it came to transformers connected to such buses. If these transformers were full-wound transformers, then no additional action had to be taken. If however they were autotransformers then exclusion of the LV buses to which they were connected meant that they would have no connection to the earth grids and that the currents in their series windings would be incorrectly calculated.

To remedy this problem an additional transformer data array called autos was created in the Excel spreadsheet. The values of this array were set to 0, 1, or 2 if the corresponding transformer was a full-wound transformer, autotransformer with an LV bus operating at 110kV or more or autotransformer with an LV bus operating at less than 110kV respectively. Functionality was then coded into runGICuniform to add the common and series winding admittances for transformers with a value of 2 in autos in series and use this admittance in a branch between the HV bus of this transformer and the substation earth grid node i.e. excluding the connection to the LV bus which is not present in the data. The array autos was also used by runGICuniform to distinguish full-wound transformers from autotransformers which were connected to LV buses operating at 110kV or greater and enter their winding admittances correctly into the admittance matrix $[Y]$.

Since buses and transmission lines of less than 110kV were not included in the study, the GICs calculated for the secondary windings of all full-wound transformers with secondaries of less than 110kV were automatically forced to zero.

4.2.2 Eliminating Dummy Buses and Bridges

The network data taken from the PSS/E fault study casefile included dummy buses for, among other reasons, representing changes in transmission line conductor types. The names of all such buses in the casefile data begin with the characters DMY. In addition to dummy buses the casefile data also included bridge buses which represent bridges between parallel feeders. Parallel feeders between the same two substations are often supported on either side of the same series of towers and are sometimes connected together at certain towers; such connections are referred to as bridges.

Neither dummy buses nor bridge buses correspond to real buses and assigning spatial coordinates to them would have been a highly time consuming task. To circumvent the problem of the unknown locations of these buses, functionality was written into runGICuniform to eliminate them and join the branches on either side of them. In order that runGICuniform could identify dummy and bridge buses it was therefore necessary to read the eight-character casefile names of all buses into the MATLAB session from the excel spreadsheet. All other buses in the network have names several characters of which resemble the name of the substation and the latter characters of which denote the voltage level and identification number of that bus. The names of dummy and bridge buses begin with the characters DMY and BRG respectively. Because of this comparative MATLAB code could readily be written into runGICuniform to identify these buses and eliminate them. The accuracy of this bus elimination functionality was confirmed using the GIC-solver package in the educational version of PowerWorld Simulator 16; this is described in a later Section.

4.2.3 Calculating the Transmission Line Equivalent Voltages due to Uniform Geoelectric Fields

In order to implement the NAM Method the quasi-DC voltages present along the transmission lines due to the uniform geoelectric fields had to be calculated. In principle the potential difference along a transmission line due to a geoelectric field must be evaluated by integrating the geoelectric field along the path which the transmission line takes [28]. This is however simple for a spatially uniform field since the potential difference between two points is independent of the path of integration; this follows naturally from the laws of vector calculus. The voltage along any transmission line between two substations due to a uniform geoelectric field can therefore be calculated by taking the dot product between the geoelectric field and the displacement vector between the substations:

$$V_{AB} = \mathbf{r}_{AB} \cdot \mathbf{E} \tag{4.1}$$

An appropriate coordinate system is established; for example with x denoting east and y denoting north.

It was therefore necessary to write code which could approximate distances across the Earth between two points specified in latitude and longitude. There were any number of methods available, but since the smallest length scales of importance in this study were kilometres, only a relatively simple method was necessary. The method chosen was the Approximate Ellipsoidal Method. The formulae for implementation of this method were taken from a publicly available spreadsheet downloaded from the Geodetic Calculation Methods page of the Geoscience Australia website. Geoscience Australia is a prescribed agency of the Australian government and was hence trusted as a reliable source. The author acknowledges Geoscience Australia for the provision of these formulae among other things.

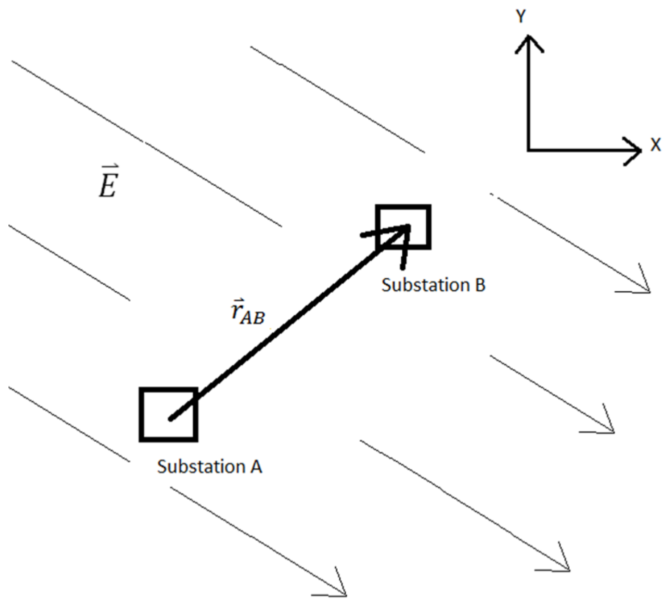

Figure 4.3: The displacement vector between two substations

According to Geoscience Australia the constants present in the formulae of this method are derived specifically for use in Australia and the accuracy of the formulae over 50 kilometres is approximately 200 metres. The Approximate Ellipsoidal Method formulae for calculating the distance between point A of latitude θ_A and longitude δ_A and point B of latitude θ_B and longitude δ_B combined into one equation yield:

$$\|\mathbf{r}_{AB}\| = \left\| \frac{111.08956(\theta_B - \theta_A + 10^{-6})}{\cos\left(\arctan\left(\cos\left(\theta_A + \frac{1}{2}(\theta_B - \theta_A)\right)\frac{(\delta_B - \delta_A + 10^{-6})}{(\theta_B - \theta_A + 10^{-6})}\right)\right)} \right\| \tag{4.2}$$

Source: Geoscience Australia [48]

Note that the latitudes and longitudes in Eq. (4.2) must be specified in decimal degrees and not radians. A MATLAB function called coordinatestodistance was written to implement this equation and this function was in turn used in runGICuniform to calculate the distances between substations. The voltages V_{GMD} required by Eq. (2.1) for implementation of the NAM Method were then calculated using Eq. (4.1).

This function was also used to test the accuracy of the spatial data collected for the substations and transmission line tees. The PSS/E casefile from which the network topology information was acquired also contained approximate lengths of the transmission lines between substation buses and tee buses. All lengths calculated by coordinatestodistance were checked against these approximate lengths and any

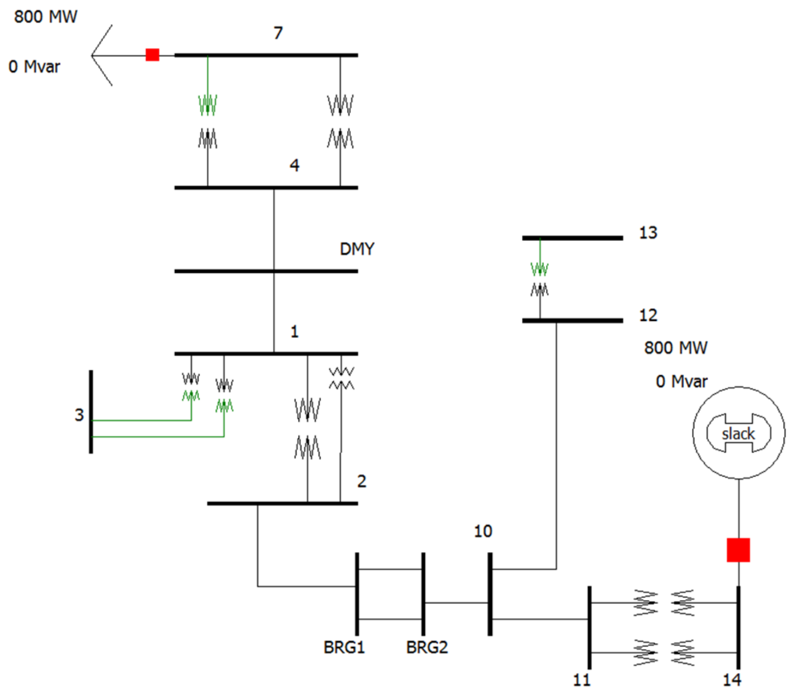

Figure 4.4: Test System in PowerWorld

substantial differences were investigated for errors in coordinates. Several errors in the locations of substations were identified and rectified in this way. Functionality was also written into runGICuniform to raise an error if any bus coordinates had values of zero; this is a common error when importing data from an Excel spreadsheet into a MATLAB session.

4.3 Verification of runGICuniform via PowerWorld

In order to verify runGICuniform produced the correct results, a hypothetical power system of sufficient complexity was created in the freely downloadable educational version of the commercial software PowerWorld Simulator 16. The latest version of this software comes with a GIC-solving tool which can solve the GIC distribution in a power network given specified geoelectric fields. The test system which was created within the PowerWorld Simulator 16 environment is displayed in Fig. 4.4. Note that a load and generator are only present in the system because PowerWorld requires that both of these be present in order to perform any simulations.

The test system contained the maximum number of buses permitted by the educational version of this software. Note the presence of two bridge buses and one dummy bus; the system was given these to test the functionality of runGICuniform which eliminated such buses from the calculation. Of the nine transformers included in the test system, six of them were autotransformers and three of them full-wound transformers. All transformers were given different winding resistances. Though it is not evident in Fig. 4.4, the test system consisted of four substations; each of these were given different earth grid grounding resistances.

Buses 3, 7, 13 and 14 had operating voltages below 110kV. Setting the voltages of these buses at these values was intentional; this allowed testing of the ability of runGICuniform to correctly calculate the GICs in the HV windings of transformers which were connected to LV buses of operating voltages below 110kV. Some of the transformers connected to these buses were made to be autotransformers while others were made to be full-wound, so as to test the ability of runGICuniform to correctly calculate the HV winding GICs for both.

A geoelectric field of magnitude 1V/km and inclination 45 degrees counter-clockwise of east was applied to the test system in PowerWorld Simulator 16 and the resulting transformer winding GICs are shown in Table 4.1. A spreadsheet of network data corresponding to the test system which was created in PowerWorld was made and loaded into a MATLAB session. The GIC distribution which would be generated by the same geoelectric field which was entered into the PowerWorld simulation was then calculated using runGICuniform. The calculated transformer winding GICs were then divided by three, since runGICuniform calculates the total of the three phase GICs in each winding while the convention of the PowerWorld Simulator GIC tool is to calculate the single phase GICs. The transformer GICs calculated by runGICuniform were then also multiplied by negative one since the convention in the runGICuniform is to define GICs flowing into the transformer windings from the network and towards the neutral as positive while the PowerWorld software has the opposite convention.

The results of the transformer winding GICs in the test system calculated by runGICuniform are displayed next to the PowerWorld results in Table 4.1. Note that all results in this table are displayed in amperes per phase.

The close agreement between the results is clear and was taken as sufficient verification of the accuracy of runGICuniform. It should be noted that some small disagreement is expected due to the fact that PowerWorld Simulator uses a method different to the Approximate Ellipsoidal Method used by runGICuniform for the calculation of distances between two points of specified latitude and longitude.

Table 4.1: Comparison of test system results calculated using PowerWorld Simulator and Code (i.e. runGICuniform)

PowerWorld HV Winding GICs	PowerWorld LV Winding GICs	Code HV Winding GICs	Code LV Winding GICs	From Bus No.	To Bus No.
-2.538	-2.538	-2.535	-2.535	14	11
-0.124	0.000	-0.125	0.000	3	1
2.483	2.483	2.491	2.491	7	4
-4.278	1.152	-4.290	1.152	1	2
2.262	2.262	2.270	2.270	7	4
-2.538	-2.538	-2.535	-2.535	14	11
-0.954	-0.954	-0.973	-0.973	12	13
-0.124	0.000	-0.125	0.000	3	1
-0.220	0.601	-0.222	0.601	1	2

4.4 Code for GIC Calculations given Non-uniform Fields

Another goal of the project was to calculate the GIC distributions flowing in the network due to geoelectric fields which are not spatially uniform. In principal this requires solving line integrals of the geoelectric field along the paths of each transmission. However, the length scales of significant directional variations of practical geoelectric fields are much greater than the length scales over which significant variations in transmission line directions occur. The approximation of such line integrals as summations of dot products between short subsections of transmission lines and the average geoelectric fields over those subsections was therefore considered to be of sufficient accuracy. In other words, for a transmission line between substations A and B, with N subsections between which significant variations in direction occur and where the displacement vectors of each subsection are denoted by $\mathbf{l_i}$:

$$V_{AB} = \int_A^B \mathbf{E}(\theta, \delta) \cdot \mathbf{dl} \approx \sum_i^N \mathbf{E}(\theta_i, \delta_i) \cdot \mathbf{l_i} \tag{4.3}$$

Note that $\mathbf{E}(\theta, \delta)$ is the geoelectric field at latitude θ and longitude δ and hence $\mathbf{E}(\theta_i, \delta_i)$ is the value of the field below the middle of subsection i. In order to use Eq. (4.3) to estimate the potentials induced along transmission lines in the network by non-uniform geoelectric fields, the coordinates of the beginning and end of each subsection or span of each transmission line in the network were acquired. A MATLAB function called runGICnonuniform was then written to apply Eq. (4.3) to these spans one by one and sum their effects over each transmission line.

Unfortunately the span data could not be acquired in a form where the order of the spans was indicative of the succession of spans in each transmission line. A number indicating which transmission line that each group of spans were subsections of, known as the feeder number, was however available. The numbers of the buses at either end of the transmission line which each span was a subsection of were also available. Within each transmission line however, the order of the spans was not known beforehand. This order had to be established for each transmission line by iterating over each span and searching for the next nearest span in the list for that transmission line. Application of this functionality revealed some apparent errors in the span data; at times the final span in a group of spans for a given transmission line would be at a location of excessive distance from the bus which the line was meant to end at, or distances between spans within the line were excessive. In both cases the only option was to abandon the span data for that transmission line. Unfortunately this meant that the span data for a large fraction of the transmission lines in the network could not be used.

Where span data could not be used or was not available for a particular transmission line, the geoelectric field was integrated along the shortest possible path between the two buses at either end of the line i.e. a straight line given the assumption of a flat Earth. This estimation was carried out by simply applying Eq. (4.3) to this straight line path with the geoelectric field re-evaluated every 500 metres. This salvaged some accuracy in the attempt to integrate all transmission lines with the geoelectric fields since the paths of many of the transmission lines in the network are likely to be reasonably close to straight lines.

4.4.1 Verification of runGICnonuniform via Comparison of Results for Uniform Fields

The spatial-integration functionality of runGICnonuniform was tested by applying randomly generated uniform fields to it and comparing results from it with those of runGICuniform. Errors in the application of Eq. (4.3) of any kind would produce incorrect summations and hence would not correctly reproduce the voltages induced along the transmission lines due to the uniform geoelectric field. Hence, this was considered a sufficient test of the code.

Unfortunately the non-uniform geoelectric field code does not reproduce the GIC

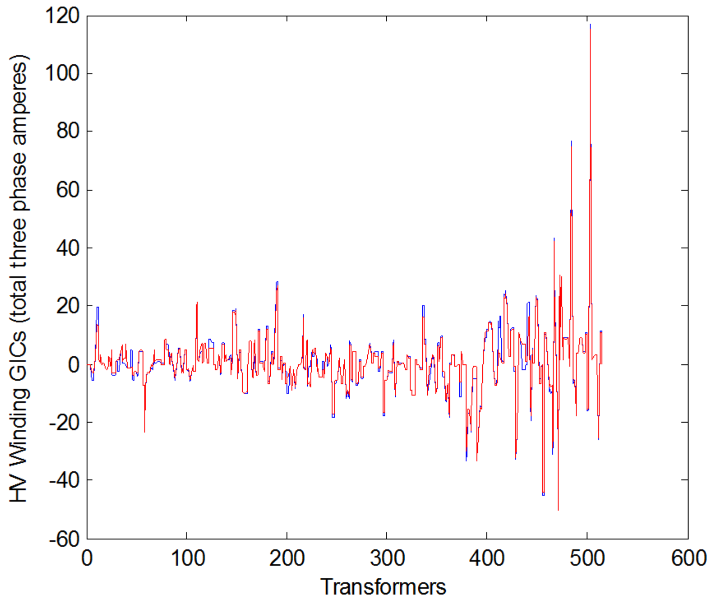

Figure 4.5: Comparison of HV winding GICs estimated by runGICuniform (blue) and runGICnonuniform (red) given a uniform geoelectric field

distribution of the uniform geoelectric field code with total accuracy. Fig. 4.5 demonstrates the scale of the errors which are produced for a randomly generated uniform geoelectric field. The blue plot is the HV winding GIC produced by runGICuniform, the red plot is the same generated by the runGICnonuniform.

Though the agreement would seem unsatisfactory, it was demonstrated that the particular transformers for which there is a significant disagreement between runGICuniform and runGICnonuniform given uniform geoelectric fields are independent of those geoelectric fields. The differences between the HV winding GICs for each transformer estimated by runGICuniform and runGICnonuniform for a randomly-generated uniform geoelectric field were calculated and then normalized by dividing by the maximum HV winding GIC predicted by runGICuniform. These are referred to generally as the GIC error for each transformer. The GIC errors for each transformer were re-calculated twenty times for twenty different randomly generated uniform geoelectric fields and the root mean squares of these are plotted in Fig. 4.6.

If the GIC error for each transformer were a function of the geoelectric field then the plot in Fig. 4.6 would be relatively flat. The fact that it is not indicates that the GIC error for each transformer is not related to the uniform geoelectric field. In other words the transformers for which runGICnonuniform calculates the winding GICs with significant error are always the same, and relatively few at that. The mean of the root mean square GIC errors is approximately 0.0106 or 1.06%. It can therefore be said in general that although there are errors in the GIC estimations produced

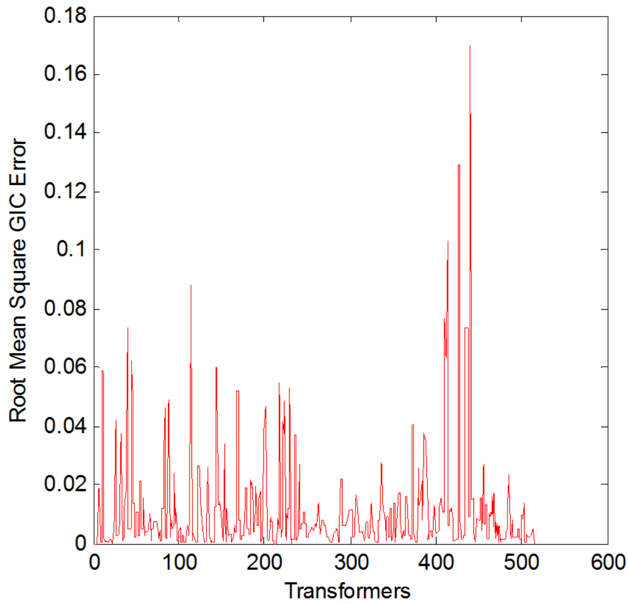

Figure 4.6: Root mean square GIC error from twenty different randomly generated uniform geoelectric fields

by runGICnonuniform, even the largest of these, which occur for a small number of transformers in the system, are only around 15% of the maximum magnitude of GIC in the network. Despite these small inaccuracies, runGICnonuniform was considered sufficiently accurate for use in comparing the GIC distributions in the network driven by uniform and non-uniform geoelectric fields.

4.5 Geomagnetic Data Collection and Processing

4.5.1 Geomagnetic Data Sources

Geomagnetic data used in this project were downloaded from the website of the Ionospheric Prediction Service or IPS, a branch of the Bureau of Meteorology, which is a department of the Australian Government. The IPS is acknowledged in this thesis for providing this service.

The IPS website provides access to magnetometer readings from several magnetometers in and around Australia. For the most part, the stations at Darwin, Townsville and Culgoora were used to interpolate geoelectric field estimations to locations across Queensland. The methods with which these estimations were made and with which they were interpolated are discussed in later Sections of this thesis. Occasionally the data recorded at the Culgoora magnetometer station were unreliable; in such circumstances data from the Canberra magnetometer station was used. Since Darwin is located in the Northern territory far to the west of Queensland and both Culgoora and Canberra are south of Queensland, it was imperative to have the Townsville geomagnetic data so that the interpolations were reasonably accurate for locations inside Queensland.

For a particular study later in this thesis historical geomagnetic data recorded at magnetometer stations at Birdsville and Weipa, two locations in Queensland, were provided by staff of the International Centre for Space Weather Science and Education based at Kyushu University in Japan [34]. The author would like to thank Professor K. Yumoto of Kyushu University in particular for provision of this data.

4.5.2 Interpretation of Magnetometer Readings

Data files downloaded from the IPS website contained data in a format which was simple to import into MATLAB as arrays. The general format was:

hh mm ss HH DD ZZ

Note that hh, mm and ss refer to the hour, minute and second at which the data was recorded and HH, DD and ZZ refer to the value of the geomagnetic H, D and Z components at that time in units of nano-Tesla. All geomagnetic data downloaded from the IPS website was downloaded directly, meaning that it was not screened nor ensured of quality by scientists in the IPS. For this reason all such data was carefully checked and analysed by the author. Several types of errors were occasionally observable in the data. At times, in the case of data from Culgoora station, it was apparent that the magnetometer unit had stopped working altogether; recording only meaningless data of a constant value. Data for days where this had occurred had to be sought from another station.

A common error was that a small number of data points would suddenly be missing. An example is shown below:

2	4	32.00	-876.017578	-7.478884	-467.468750
2	4	34.00	-875.994141	-7.529004	-467.593750
2	4	35.00	-876.017578	-7.541465	-467.617188

Note that the values of the H, D and Z components for the 32nd, 34th and 35th seconds of the fourth minute of the second hour of the day which this data is for are present, but the values for the 33rd second are missing. Simple linear interpolation code was written to deal with this problem and was applied to all geomagnetic data

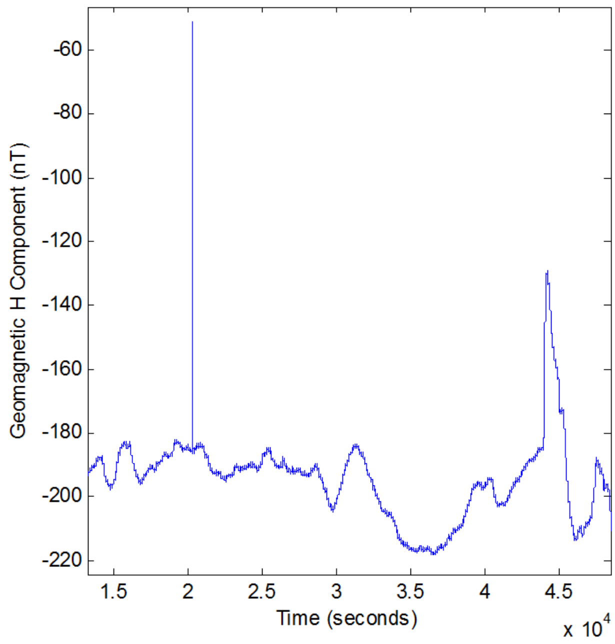

Figure 4.7: Sharp step of an SC (right) contrasted with a spike due to a data recording error (left) [47]

before they were used for geoelectric field estimation. In other words, it was assumed that all missing data points could be approximated by linear functions fitted to the data points which were present either side of the gap.

Another problem more difficult to deal with was the presence of erroneous spikes in the data. An example of this is shown in Fig. 4.7; an erroneous data spike is contrasted with the relatively sharp spike of an SC.

These spikes were identified by observing plots of all data downloaded; something which MATLAB is particularly suited to. Particular care had to be taken to identify such spikes where they were present and to distinguish them from natural rapid variations of the geomagnetic field. They were removed by smoothing them over with linear interpolations fit to values of the field components selected closely on either side of them. An example of this is shown in Fig. 4.8 where the blue plot is the geomagnetic data before the spike was removed and the red plot is the geomagnetic data after it was removed.

For certain days the data downloaded contained a prohibitive number of erroneous spikes; such data had to be neglected and replaced with data from another station for that day. Fig. 4.9 shows the D component data for the 2nd of September; data which was unusable due to excessive erroneous spikes.

In general, data was downloaded for at least two consecutive days and joined together

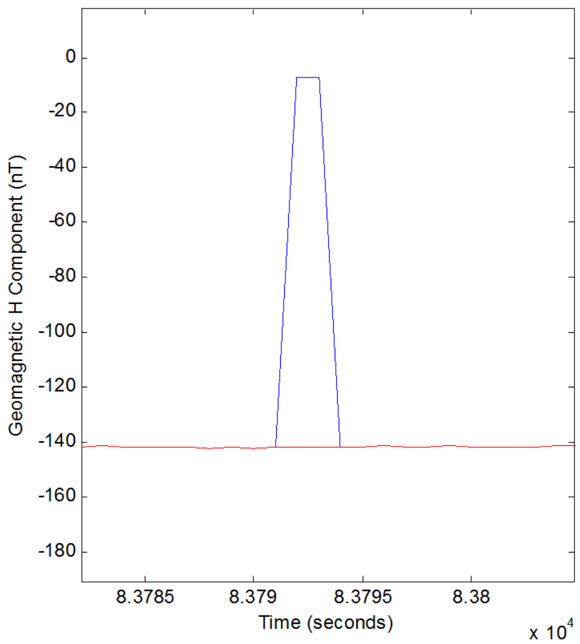

Figure 4.8: Temporal geomagnetic data before (blue) and after (red) removal of an erroneous spike [47]

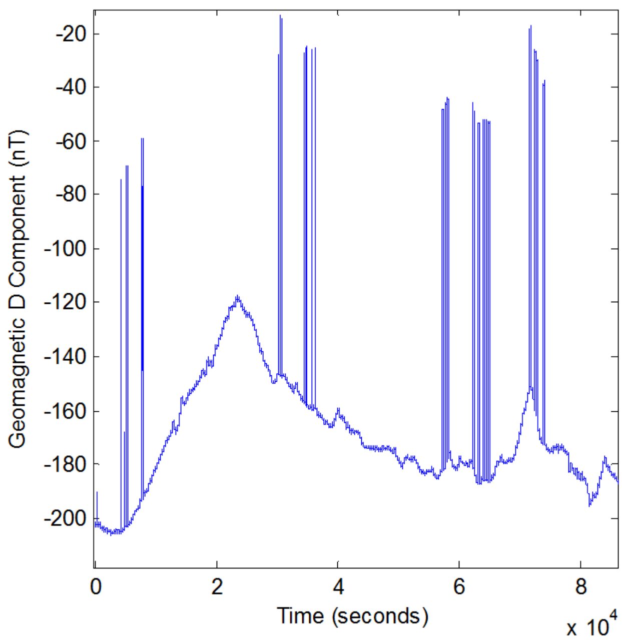

Figure 4.9: Excessive erroneous data spikes [47]

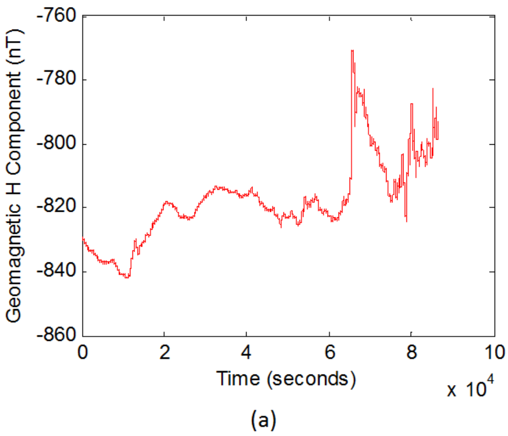

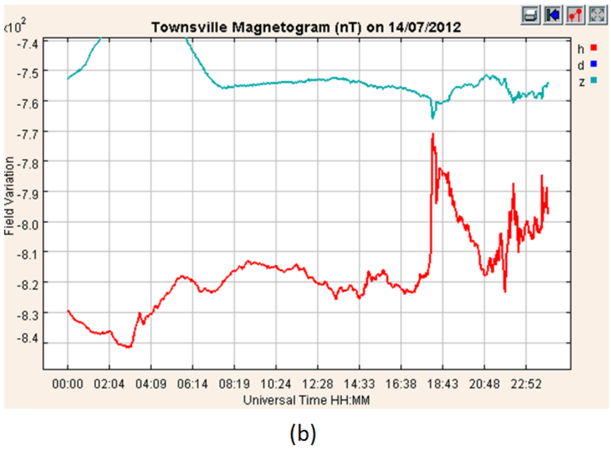

Figure 4.10: (a) Temporal geomagnetic data in the MATLAB session checked against (b) data plotted on the IPS website [47]

with appropriate vectors of seconds beginning on the first day. Often the data files would not contain data for the last few minutes or seconds of a day; data downloaded from the Darwin magnetometer were consistently missing data points for the last three minutes of each day. In such circumstances the data had to be filled out using the same linear interpolation procedure that was applied to gaps in the data.

As a final check that the correct data had been downloaded, all data sets were checked against plots of the data provided on the IPS website. Fig. 4.10 shows the comparison for the H component data on the 14th of July 2012.

4.6 Estimating Geoelectric Fields with Geomagnetic Data

In order to estimate GIC distributions in the Queensland power transmission network a method was required with which to estimate geoelectric fields induced during space weather disturbances. During the initial stages of the project it was intended to use the spectral domain method described in Subsection 2.2.1 of Chapter 2. Implementing this model showed some positive results but also others which were somewhat erroneous; the author does not believe it to be a shortcoming of the work developed by [33], but rather a failure to correctly implement it in this project. In any case, the temporal domain method was adopted later in the project; the reasons for this are explained in Subsection 4.6.3 of this Chapter.

The implementation of both the spectral domain method and the temporal domain method are described in the following two Sections.

4.6.1 Implementation of the Spectral Domain Geoelectric Field Estimation Method

The first step in implementation of the spectral domain method was to apply a discrete-time Fourier transform to temporal geomagnetic data to put it in the frequency domain. In this thesis the basic fft function in MATLAB was used to achieve this. As previously mentioned, all geomagnetic data used was measured at a sampling frequency of 1Hz. This means that the data had a Nyquist frequency of 0.5Hz and hence any spectral components of the geomagnetic data of frequencies greater than this had to be neglected. Variations with a frequency of 0.5Hz or greater are not of interest in the studies which were considered in this project; the fundamental frequencies present in SCs generally have periods on the order of minutes [36] and those of geomagnetic sub storms have greater periods than this.

The fft function in MATLAB produces an array which represents the time domain signal given to it against frequencies ranging from 0Hz to the Nyquist frequency and back to 0Hz. The number of frequencies at which a term in the Fourier domain exists depends on the number of temporal data points with which the fft function is called. In general, for N temporal data points frequency f_n of the Fourier domain array is given by:

$$f_n = \frac{mf_s}{N} \tag{4.4}$$

Note that f_s is the sampling frequency and that m ranges from 1 to $N/2$ and then from $N/2$ back to 1 because the Fourier domain representation of the signal is folded symmetrically either side of the Nyquist frequency. In other words:

$$n = 1, 2, 3 \ldots N \tag{4.5}$$

$$m = 1, 2, \ldots \frac{N}{2} - 1, \frac{N}{2}, \frac{N}{2}, \frac{N}{2} - 1 \ldots 2, 1 \tag{4.6}$$

Note also that:

$$f_{N/2} = f_{N/2+1} = \frac{1}{2} f_s \tag{4.7}$$

It was therefore necessary to have an even number of data points; one temporal data point was neglected if the number of data points present was odd. A function called calcgeoEspectralmethod was written to apply Eq. (2.7) to Fourier domain geomagnetic data, making use of another function which was written to evaluate $\tilde{Z}_N(\omega)$ from Eq. (2.6) for the frequency of f_n of the nth temporal data point $\tilde{B}_{n,x}$ using the angular frequency:

$$\omega_n = 2\pi f_n \tag{4.8}$$

In order to apply a low pass-filter to the data, the function evaluating $\tilde{Z}_N(\omega)$ was forced to zero for frequencies greater than 0.25Hz. The MATLAB function ifft was then used to calculate the inverse-Fourier transform of $\tilde{E}_y$. This procedure was applied to the geomagnetic H component data and D component data in order to calculate the westward geoelectric field and the northward geoelectric field at the given magnetometer site respectively.

4.6.2 Implementation of the Temporal Domain Geoelectric Field Estimation Method

A function called calcgeoEtemporalmethod was written in MATLAB to apply Eq. (2.9) through to Eq. (2.11) from Subsection 2.2.2 to temporal geomagnetic data downloaded from the IPS website. The accuracy of the numerical approximation to the integral in Eq. (2.8) relies on the amount of temporal geomagnetic data prior to the time when the geoelectric field is to be calculated being sufficiently large; [38] advises at least twelve-hours worth. It was therefore consistently ensured that when the geoelectric field during a particular event was estimated, the geomagnetic data used to perform that estimation was for the day of the event as well as the day which preceded it. As an example, to estimate the geoelectric field during the SC of the 14th of July 2012, temporal geomagnetic data for the 13th and 14th of July was downloaded and used in the calculation of the geoelectric field on the 14th of July.

The cadences of all geomagnetic data used was one second which allowed accurate calculation of the geoelectric fields induced by SCs and other geomagnetic events, since all of these generally have fundamental frequencies of orders less than 0.1Hz. The single conductivity value used when implementing this temporal geoelectric field estimation method was the inverse of the depth-weighted average of the seven resistivities in the Campbell conductivity model. The calculation of this depth-weighted conductivity is shown below:

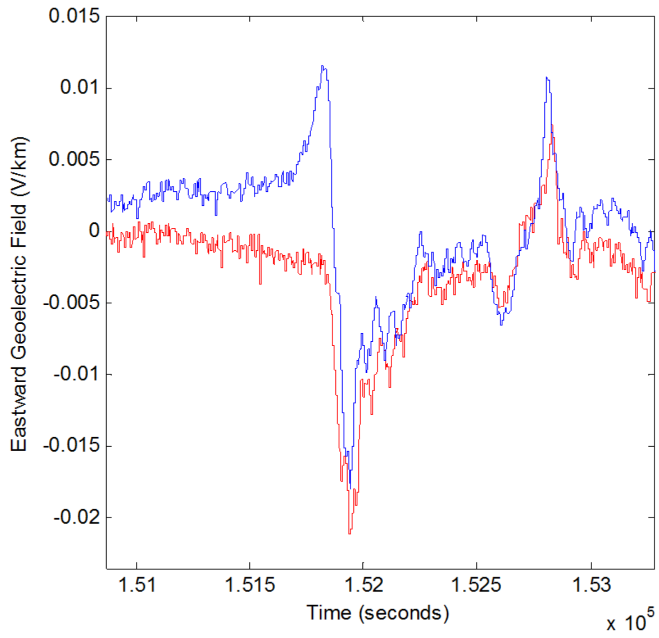

Figure 4.11: Comparison of the geoelectric field estimates produced by calcgeospectralmethod (blue) and calcgeoEtemporalmethod (red) during an SC

$$\sigma = \sum_{i=1}^{N} \frac{1}{w_i \rho_i} \tag{4.9}$$

$$w_i = \frac{d_i}{\sum_{j=1}^{N} d_j} \tag{4.10}$$

Therefore, given the layer thicknesses d_i and the resistivities ρ_i of the Campbell conductivity model:

$$\sigma = 0.03176 S/m$$

4.6.3 Inaccuracy of the Spectral Domain Geoelectric Field Estimation Method

As previously mentioned the spectral domain geoelectric field estimation method was found to produce anomalous spikes in geoelectric field estimations preceding SCs for unknown reasons. A plot of the eastward geoelectric field estimations for the SC of the 14th of July is shown in Fig. 4.11. The red plot is the geoelectric field calculated by calcgeoEtemporalmethod and the blue plot is the geoelectric field

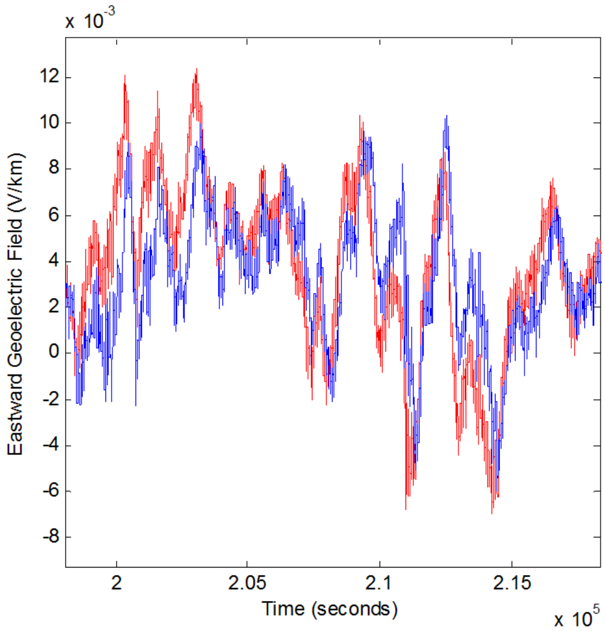

Figure 4.12: Comparison of the geoelectric field estimates produced by calcgeospectralmethod (blue) and calcgeoEtemporalmethod (red)

calculated by calcgeoEspectralmethod. Note the anomalous spike in the estimation by the latter.

At other times however there is clear correlation between the geoelectric fields estimated via both methods, though there is also often some offset between them. Fig. 4.12 shows an example of such correlation.

The agreement between the two functions was taken as verification that the estimaitons produced by calcgeoEtemporalmehtod were of the right order of magnitude in general; an important confirmation as this was expected to be a rather inaccurate method.

Though the spectral domain surface impedance method implemented by [33] produce estimations of superior accuracy to the temporal method of [38], it was decided that the former could not be used with confidence. The reasoning for this was that it was a more complex method to implement and was clearly producing some strange results, whereas the latter method was relatively simple in comparison and it was considered unlikely that errors had been made in its implementation.

4.6.4 Interpolating Geoelectric Field Estimations

In order to estimate the geoelectric fields at different locations around Queensland it was necessary to assume smooth variations of the fields between the locations where they were initially estimated, namely the magnetometer locations. MATLAB code was written to implement a smooth interpolation procedure where the influence of the geoelectric field estimation at each magnetometer site on the geoelectric field estimation at the new location is weighted by the inverse of the distance between the site and the new location.

Let the latitude and longitude of a new location where values of the geoelectric field are to be estimated be denoted by and respectively. The values of the geoelectric field at this new location, both the northward and eastward components thereof, can therefore be referred to generally as $E(\theta, \delta)$. Let the number of magnetometer sites be N and let the estimated geoelectric field values at these sites be denoted generally by E_i. Let w_i denote the weight of E_i on $E(\theta, \delta)$. Then assume that:

$$E(\theta, \delta) = \sum_{i}^{N} w_i E_i \tag{4.11}$$

Let the weight w_i be given by:

$$w_i = \frac{\frac{1}{r_i}}{\sum_j^N \frac{1}{r_j}} \tag{4.12}$$

The variable r_i is the distance from the new location (θ, δ) to the location of magnetometer site i. Note that the weights are automatically normalized so that:

$$\sum_{i}^{N} w_i = 1 \tag{4.13}$$

MATLAB code was written to solve Eq. (4.11) and Eq. (4.12) for any given coordinates (θ, δ) for both the northward and eastward components of the geoelectric field. This function was then used within other functions to evaluate the geoelectric fields at locations across the network once they had been evaluated at the magnetometer sites using either the spectral domain estimation method or the temporal domain estimation method.

4.7 Modelling the Geomagnetic Coastal Effect

Later in this thesis, it became necessary to model the geomagnetic coastal effect. In the discussion that follows the unit vectors $\hat{u}$ and $\hat{v}$ denote the directions which are perpendicular to and parallel with the coastline respectively. The entire Queensland power transmission network is situated against the eastern Queensland coastline, hence the convention was adopted that $\hat{u}$ should always point in the direction more east than west (i.e. towards the ocean) and $\hat{v}$ in the direction more north than south (i.e. up the Queensland coastline).

Equations (23) and (28) from [29] were adapted to model this geophysical phenomenon. These equations are reproduced below.

$$V_u = \frac{2\mu_0^{1/4} x^{1/2}}{\sigma^{3/4}\pi^{1/2}\Gamma(3/4)} \int_0^t \frac{1}{(t-t')^{1/4}} \frac{\partial H_0(t')}{\partial t'} dt' \tag{4.14}$$

$$E_v = \frac{\mu_0^{3/4} x^{1/2}}{\sigma^{1/4}\Gamma(1/4)} \int_0^t \frac{1}{(t-t')^{3/4}} \frac{\partial H_0(t')}{\partial t'} dt' \tag{4.15}$$

Note that the subscript indicates the direction while the variable V in Eq. (4.14) is a voltage. It was assumed that the term on the left hand side of Equation (23) was a real voltage and hence could be differentiated to yield an inverse dependence on the square root of the distance inland i.e.:

$$E_u = \frac{\partial V_u}{\partial x} \sim \frac{1}{\sqrt{x}}$$

Eq. (4.15) on the other hand is an electric field, specifically the component which is parallel to the coastline, and involves a direct proportionality to the square root of the distance inland.

In order to apply these equations to the network it was obvious that runGICnonuniform would have to be applied, hence these two expressions and the temporal convolution integrals therein would have to be evaluated for every span in the network. Unfortunately the time taken to execute code performing this calculation would have been prohibitive. It was also found that the part of the integrand in Eq. (4.14) which has an exponent of -0.25 has an extremely long temporal tail; in other words the values of $(t - t')$ for which the integrand becomes negligible are far greater than one day. To estimate the geoelectric fields produced using this Equation would therefore require temporal data for several days before the event of interest.

Therefore Eq. (4.14) and Eq. (4.15) were simplified further, with the former differentiated with respect to x, such that they both contained only one and the same free variable:

$$E_u = \frac{\alpha E'_u}{\sqrt{x}} \tag{4.16}$$

$$E_v = \frac{E'_v \sqrt{x}}{\alpha} \tag{4.17}$$

Note that E'_u and E'_v are the $\hat{u}$ and $\hat{v}$ components of the horizontal geoelectric field as they would be in the absence of the coastline. They were evaluated using calcgeoEtemporalmethod and interpolategeoE. Although the combined values of the constants and integrals in Equations (23) and (28) in [29] will always have different values, one expects that the distance over which E_v is reduced should be similar to the distance over which E_u is enhanced. Eq. (4.16) and Eq. (4.17) ensure that at each point moving inland from the coastline the reduction which is applied to E'_v is the inverse of the enhancement which is applied to E'_u.

The term is hereafter referred to as the coastal coefficient. Using this variable the strength of the coastal effect and the average distance inland over which its influence extends can be freely varied. Due to the extreme simplifications which were employed to produce Eq. (4.16) and Eq. (4.17); the dependence on the temporal history of the geomagnetic field has been removed as has all conductivity information; they could only be expected to produce semi-qualitative estimates of the distributions of GICs in the Queensland network.

A function called coastalgeoE was written to evaluate the geoelectric field at a given position in Queensland with the influence of the coastal effect taken into account. To apply Eq. (4.16) and Eq. (4.17) at any given point the shortest distance x from that point to the coastline was required. A function called nearestcoastlinepoint, described in the following Section, was written to find this for any position within Queensland or northern New South Wales. For values of x great enough that $E_u < E'_u$ or equivalently $E_v > E'_v$, coastalgeoE was made to return E'_u and E'_v. In other words for a given value of the coastal coefficient there is a distance inland beyond which the coastal effect does not persist. The function coastalgeoE was incorporated into runGICnonuniform such that it was used to interpolate geoelectric field values at the location of each span in place of interpolategeoE (although coastalgeoE itself makes use of interpolategeoE).

It should be noted that the application of Equations (23) and (28) in [29] necessitates the assumption that the coastline varies negligibly in direction so that spatial symmetry in the direction up the coast is maintained. This is necessary for the validity of the two dimensional model within which all equations in [29] are derived. Over length scales of ten kilometres or more the Queensland coastline varies in direction relatively slowly; this was relied upon in the application of Eq. (4.16) and Eq. (4.17) in estimating the influence of the coastal effect.

4.7.1 Finding the Shortest Distance to the Queensland Coastline

In order that coastalgeoE could evaluate Eq. (4.16) and Eq. (4.17) at any point in Queensland the shortest distance to the coastline was required. A function called nearestcoastlinepoint was written to achieve this. The coordinates of a series of points along the Queensland coastline and part of the coastline of northern New South Wales, referred to as coastal landmarks, were specifically selected so that they were all at least 50 kilometres apart. This was done with the intention of smoothing over bays, points and other small scale geographic structures along the coastline and so that the effective angle of the coastline varied slowly. Once these coastal landmarks had been recorded using spatial software maintained by PLQ, code was written which would make use of coordinatestodistance and find the closest three of these landmarks to the point inland specified in the call of nearestcoastlinepoint. Functionality was then written to interpolate these three landmarks with a series of six thousand points and find the closest of these to the specified point inland, which the function then returns the coordinates of.

4.7.2 Verification of Code for Estimating the Coastal Effect

It had to be verified that no errors had been made in the coding of coastalgeoE or nearestcoastlinepoint, such as simple errors in trigonometry. To perform this verification, two additional and fictitious coastal landmarks were selected both with the same longitudes as the southernmost point selected previously but with ten and twenty additional degrees of southward latitude respectively. The intention was to simulate a long coastline with an angle ninety degrees counter-clockwise of east, so that the eastward and northward geoelectric fields would be equivalent to E_u and E_v respectively. The non-coastal northward and eastward geoelectric field components were set to values of -1V/km everywhere. The northward and eastward geoelectric fields which would be present with the coastal effect taken into account were estimated using coastalgeoE for several thousand points starting at the coastline and moving towards a total of one thousand kilometres inland. A coastal

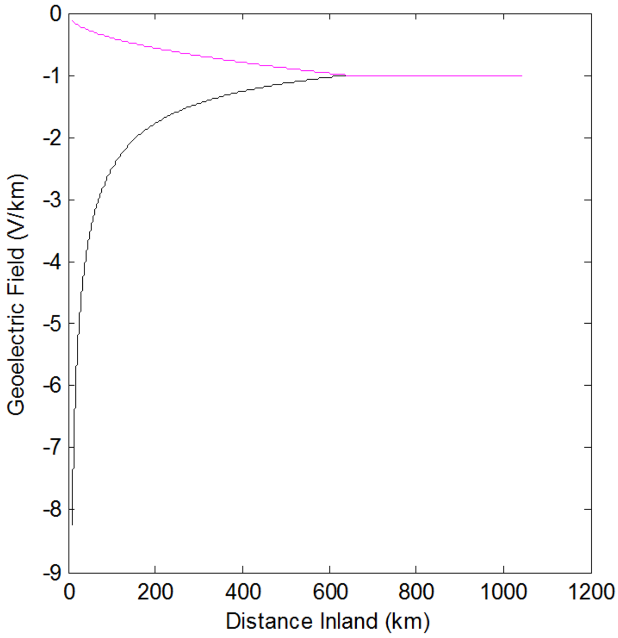

Figure 4.13: Northward geoelectric field component (pink) and eastward geoelectric field component (black) against distance inland calculated by coastalgeoE while moving westward from a coastline of northward orientation

coefficient of 800 was used. The plot of the geoelectric field estimations produced is show in Fig. 4.13.

The plots confirm the correct functioning of both nearestcoastlinepoint and coastalgeoE. The eastward geoelectric field component is completely perpendicular to the coastline, hence it is expected that its magnitude should be enhanced in the vicinity of the coastline and slowly decline with distance inland eventually settling smoothly to the non-coastal value. The black plot in Fig. 4.13 clearly exhibits this behaviour. The northward geoelectric field component is completely parallel with the coastline and so its magnitude is reduced to zero at the coastline and smoothly increases with distance inland, settling eventually at the non-coastal value. Again this is the behaviour which is expected if Eq. (4.16) and Eq. (4.17) have been applied correctly.

Chapter 5

GIC Calculation Results and Discussions

5.1 Results for Uniform Geoelectric Fields

The first study of this thesis was the calculation of the GICs which would be present in the network for hypothetical uniform northward and westward geoelectric fields of magnitude 1V/km.

The effective GIC discussed in Section 2.4 of Chapter 2 was used to present and compare all transformer GIC results in this thesis for the reasons discussed in that Section. Note also that unless stated otherwise all GIC values mentioned in this thesis are total three phase values, i.e. the sum of the GICs flowing in each of the three single phase windings.

Tables 5.1 and 5.2 display the transformers with the top twenty effective GICs for uniform 1V/km westward and northward geoelectric fields respectively. The complete results for every transformer in the network are shown in Appendix A. Note that a system of 726 unique random numbers was generated so that a code could be used to discuss each substation and transformer studied in this project without revealing the locations of equipment belonging to PLQ or other companies. Codes which are prefixed with the string SUB refer to substations while codes which are prefixed with the string TX refer to transformers.

As expected the GIC distribution is highly different for uniform northward and westward geoelectric fields. Fig. 5.1 highlights the difference between the GIC distributions for northward and westward uniform geoelectric fields by displaying the effective GICs for both graphically. The GICs for the uniform westward 1V/km field

Table 5.1: Highest twenty effective GICs for a uniform 1V/km westward geoelectric field

Transformer Name	Effective Winding GIC (total three phase amperes)
TX8010757	115.0731
TX9294844	46.4316
TX4095149	46.4316
TX3414	36.0373
TX7448678	34.1065
TX8922671	34.0482
TX9748361	33.9742
TX759673	33.9742
TX2933679	32.9744
TX1628989	31.8636
TX348657	31.45
TX3093692	31.366
TX3990752	27.5824
TX5464018	26.6521
TX3565036	26.2569
TX7461479	26.0843
TX3325714	25.0324
TX2347826	24.9583
TX8530636	24.784
TX1548287	24.6494

are displayed in red and those for the uniform northward 1V/km field are displayed in blue. Note that the horizontal axis simply represents different transformers in the network in an arbitrary order; this is true of several of the plots in this Chapter.

Since GICs are treated as DC currents, the GICs which would be present in the Queensland network as a result of any uniform geoelectric field can be calculated via superposition of the results for the uniform northward and uniform westward fields. In such a calculation however the polarity of the effective GICs would be important.

During SCs which have occurred this year, the eastward component of the geoelectric fields has shown a tendency to be an order of magnitude stronger than the northward component. Also, the northward geoelectric field component tends to vary in direction i.e. positive or negative, whereas the eastward component is

Table 5.2: Highest twenty effective GICs for a uniform 1V/km northward geoelectric field

Transformer Name	Effective Winding GIC (total three phase amperes)
TX2329815	88.0681
TX5324264	87.375
TX8010757	57.5452
TX3554071	49.0377
TX8410863	39.8761
TX3545062	39.8761
TX8928333	34.9072
TX9575431	34.252
TX7458749	30.2123
TX1255362	29.3627
TX8223940	28.8641
TX470777	28.7741
TX1628989	27.9019
TX9993294	27.8858
TX251505	27.834
TX3978391	27.6006
TX8463728	27.5265
TX8384057	27.4262
TX5588205	26.5486
TX9911877	26.3815

consistently negative i.e. westward. This is the indication from the eastward and northward geoelectric field component values shown in Table 5.3. These values were estimated using geomagnetic data recorded at Townsville magnetometer station for three SCs this year during the moments when the overall geoelectric fields were the most intense. Note that these geoelectric fields were calculated with the depth-weighted average of the Campbell conductivity model discussed in Subsection 4.6.2 of Chapter 4.

It is of course possible that geoelectric fields in mid to low-latitude regions generated by SCs could show behaviour different to that which was captured in this small sample. In light of this apparent tendency of SC-generated geoelectric fields however, the transformer winding GICs for a uniform westward field shown in Table 5.1 should be regarded as more important for the Queensland network than those for a uniform

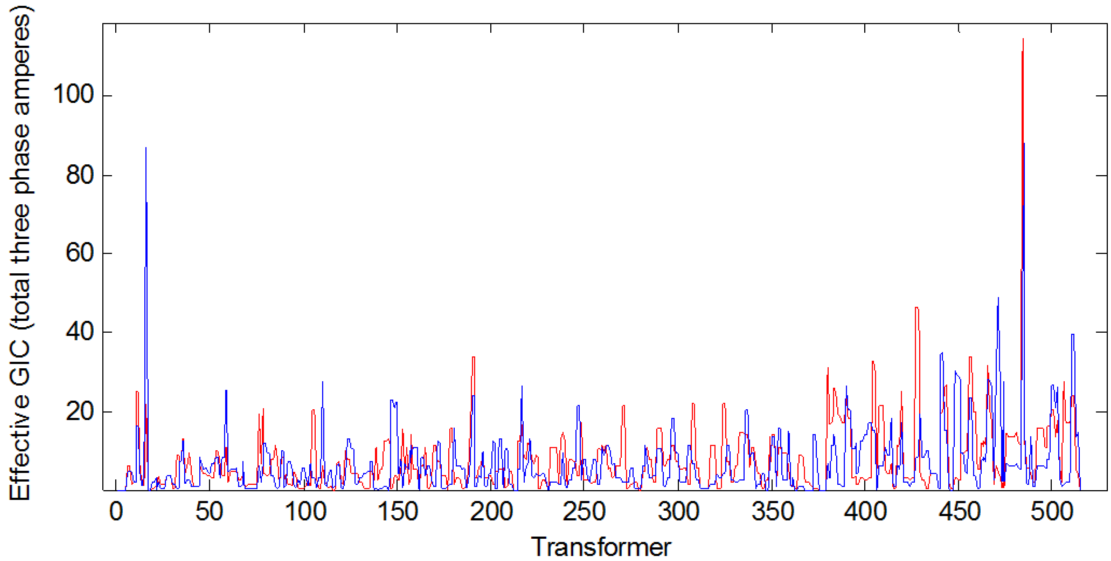

Figure 5.1: Comparison of effective GICs for uniform 1V/km northward (red) and westward (blue) geoelectric fields

Table 5.3: Estimations of geoelectric field components at Townsville for a sample of SCs in 2012

Date of SC	Eastward Geoelectric Field Component (V/km)	Northward Geoelctric Field Component (V/km)
14.07.2012	-0.0187	0.0025
12.03.2012	-0.0206	-0.0071
03.09.2012	-0.0189	-0.0023

northward field shown in Table 5.2.

5.1.1 Investigation of Geoelectric Field Orientation Importance for a Large Network

It is interesting to pose the question of whether the network is more susceptible to northward or southward geoelectric fields than westward or eastward ones. Since the Queensland power transmission network supplies cities, towns and suburbs which tend to hug the coastline and hence many of the lines span greater distances from north to south than from east to west, one might expect that they do. Fig. 5.2 depicts the largest one hundred effective GICs from the uniform geoelectric field studies assorted in ascending order. The red plot is for a uniform westward geoelectric field of 1V/km and the blue plot is for a uniform northward geoelectric field of 1V/km.

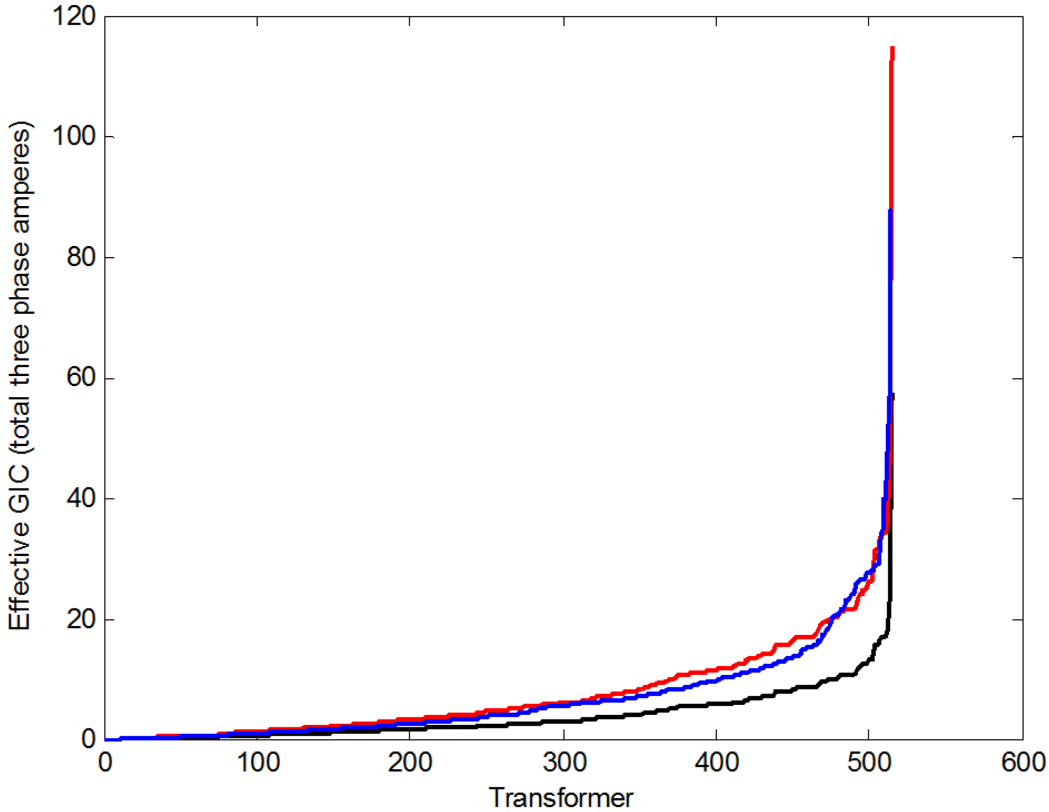

Figure 5.2: Effective GICs for uniform 1V/km westward (red), 1V/km northward (blue) and 0.5V/km westward (black) geoelectric fields assorted in ascending order

The black plot is for a uniform westward geoelectric field of 0.5V/km.

Save for the highest value in the westward geoelectric field case, the levels of effective winding GICs for the uniform 1V/km northward geoelectric field do not seem to be significantly greater than those present for the uniform 1V/km westward geoelectric field. In fact the mean value of effective GIC was 6.8441 amperes for the northward geoelectric field and 7.4883 amperes for the westward geoelectric field. The black plot depicting the effective GICs for a uniform 0.5V/km westward geoelectric field is shown for comparison and the mean value in this case was 3.7442 amperes.

It is therefore apparent that for a power transmission network as large as the Queensland network, reducing the magnitude of the geoelectric field by a factor of one half has a far greater impact on the total amount of GICs in the network than changing the orientation of the field.

5.1.2 Investigation of the effect of Critical Feeder Removal on the GIC Distribution

Since SCs tend to generate stronger westward geoelectric fields, an effective mitigation strategy might be to open circuit key transmission lines in the network which run long distances from east to west. To investigate the effectiveness of such a strategy, a brief study has been conducted where four such feeders have been removed from the network; two feeders running from SUB901660 to SUB3891287 and two from SUB4389896 to SUB4832945. All of these transmission lines operate at 275kV and all of them have lengths of over 100 kilometres making them relatively critical feeders in the network. They will hereafter be referred to as simply the critical feeders. The GIC distribution given a uniform westward geoelectric field was recalculated with these lines removed and the results for the largest twenty effective GICs calculated are presented in Table 5.4.

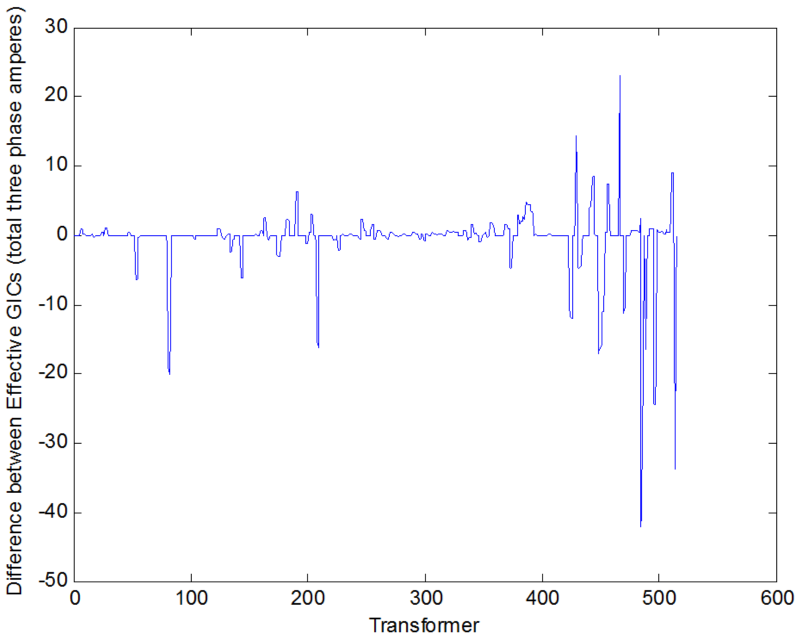

Figure 5.3: Differences in effective GICs before and after removal of the critical feeders

Comparing these results to those in Table 5.1, the hierarchy of transformers with high effective GICs has changed somewhat. Fig. 5.3 depicts the change to the distribution of GICs more effectively; it shows the differences between the effective GICs for each transformer before and after removal of the critical feeders. Note that a positive value on this plot indicates that removal of the feeders resulted in a reduction of effective GIC, a negative value indicates an increase in effective GIC and a value of zero indicates that no change in effective GIC occurred.

Table 5.4: Highest twenty effective GICs for a uniform 1V/km westward geoelectric field with critical feeders removed

Transformer Name	Effective Winding GIC (total three phase amperes)
TX8010757	112.4536
TX2329815	58.0372
TX9294844	46.4292
TX4095149	46.4292
TX9324686	39.7952
TX5722392	38.0444
TX2904624	35.2513
TX4025543	35.2513
TX4300694	34.4529
TX2933679	32.9911
TX3093692	31.3816
TX348657	28.4742
TX9748361	27.8303
TX759673	27.8303
TX3990752	26.7467
TX7448678	26.5859
TX8922671	26.5231
TX3325714	25.0352
TX2347826	24.9585
TX8530636	24.7867

As expected, for many of the 515 transformers included in the study the change in effective GIC after removal of the critical feeders was negligible. For some of them however it was significant. Fig. 5.3 does not seem to indicate a reduction in effective GIC values, on the contrary; the predominant trend is a negative difference indicating an increase of effective GICs overall after removal of the critical feeders. The mean value of effective GIC before removal of the critical feeders was 7.4883 amperes and after their removal it increased, albeit only slightly, to 7.9956 amperes.

It is also of interest what the changes in effective GICs were for the transformers at the substations to which the four critical feeders were directly connected. Table 5.5 displays the effective GICs before and after removal of the four critical feeders for these transformers.

Save for TX1628989, removal of the critical feeders resulted in significant increases

Table 5.5: Effective GICs in transformers located at substations either end of the critical feeders before and after the critical feeders were removed

Transformer Name	Normal Network State	Feeders Removed
TX6019797	2.7051	14.4328
TX8571687	3.2561	15.1559
TX9882771	3.2561	15.1559
TX4300694	5.391	34.4529
TX5722392	4.2658	38.0444
TX1628989	31.8636	8.7555
TX2077306	2.7479	7.5465
TX3258062	0.4824	5.039
TX959494	0.4824	5.039
TX2192835	2.6673	7.5075
TX9993294	6.1727	17.391

in effective GICs for all transformers at the substations which were connected to the critical feeders. This result is in fact somewhat intuitive if one considers a simple network of transmission lines heading in only one direction. Referring to the results of Section 6 of [26], it is expected that for such a system the highest GICs will be present in the transformers on the edges of the network. This result can be extended to general transmission networks to conclude that the GIC in a given transformer is likely to be lower if it is situated in the middle of the network and higher if it lies on the edge of the network.

Removing long feeders therefore creates new discontinuities in the network, which means that the transformers at the substations to which the removed feeders were connected are suddenly situated on new edges of the network. It is therefore somewhat expected that the removal of the critical feeders will increase the GICs flowing through many of the transformers in Table 5.5. On the other hand; it is expected that removing transmission lines with east-west orientations will reduce the coupling of the network with a geoelectric field which is predominantly westward or eastward. It would be useful to conduct the study in this Section again with a greater number of feeders with east-west orientations removed from the network and see if the average effective GIC in the network is reduced for a uniform westward geoelectric field. Indeed; an interesting study would be to see if the average effective GIC exhibits a critical point with respect to the number of east-west feeders removed from the network given a uniform westward geoelectric field.

Though the distribution of GICs is significantly altered as indicated by Fig. 5.3 the change in the mean effective GIC values from 7.4883 amperes to 7.9956 amperes would seem to suggest that removal of the critical feeders would in fact result in an increase of effective GICs in the transformers of the network in general. Removal of feeders may therefore be an ineffective mitigation strategy during a severe geomagnetic storm or SC.

5.2 Results for Non-uniform Geoelectric Fields

The second goal of this thesis was to use non-uniform geoelectric fields to estimate the GICs which had occurred in the network during times of known geomagnetic activity in the latter half of the year. These estimations were to be verified against direct GIC measurements in the neutral of a transformer at SUB901660; the code for this transformer is TX5722392. The transformer chosen for application of the GIC measurement device was one with a relatively high power rating and a critical position in the southern part of the network. It was also chosen due to its position on the edge of the small part of the Queensland transmission network which operates at 330kV. This higher operating voltage was expected to ensure relatively large GIC values in this transformer during geomagnetic disturbances compared to those flowing through others in the network. The current transducer was installed on the neutral of TX5722392. Since this is an autotransformer the GICs flowing through its neutral are the same as the total three phase GICs flowing through its common winding.

The first major current spike observed in the device occurred during an SC on the 14th of July. The peak magnitude of the neutral GIC during this event was approximately -5.3 amperes. The first estimation of the GIC distribution in the network at this time using runGICnonuniform yielded a current of only -0.0187 amperes in the LV winding (common winding) of TX5722392. It was clear that the GIC estimations were out by a substantial amount; the next important step was to determine whether they were out by a relatively constant factor i.e. whether they correlated well with the measured data. This is detailed in the following Section.

5.2.1 Determination of an Error Scaling Factor for the Model

In order to determine whether the GIC estimations were out by a constant factor, specific periods over which notable GICs were measured in the neutral of TX5722392 on three separate days were selected. This constant factor was to be termed the error scaling factor of the model if it was found.

Geoelectric field estimations for the selected periods were made using calculategeoEtemporalmethod and geomagnetic data from Townsville and Culgoora magnetometer stations. These were then interpolated to the position of SUB901660 using interpolategeoE. To reduce computation time, runGICuniform was then called every four seconds over the selected periods. Calling runGICuniform over the time periods selected resulted in computation times of a few hours while calling runGICnonuniform would have resulted in computation times of several days. It was assumed that since only the GICs at SUB901660 were to be known accurately for these calculations that ensuring that the geoelectric field had the correct values at this substation was sufficient for determining the existence and value of the error scaling factor.

Each time runGICuniform was called over the selected periods the value of the GIC in the LV of TX5722392 was stored and all other results were neglected. Code was the written to multiply the GIC estimates for each period by a range of scaling factors from 10 to 25 and select the scaling factor which resulted in the lowest root mean square difference between the estimated data and the measured data when the measured data exceeded 1 Ampere. In other words the differences between the measured data and the estimated data at times when the measured GIC was less than 1 ampere were not of interest.

The scaling factors which were found and the root mean square difference between the estimated and measured data given such re-scalings are shown in Table 5.6. Note that all dates and times discussed in this thesis are in Universal Time (UTC) and note that all calculations presented in Table 5.6 have been reproduced with three significant figures as accuracy greater than this cannot be expected.

Table 5.6: Error scaling factors for three separate periods containing GIC spikes

Date (UTC)	Time Period of Estimation (UTC)	Maximum Measured Neutral GIC Magnitude (Amperes)	Error Scaling Factor	RMS Difference (Amperes)
14.07.2012, 15.07.2012	14:53:20 (14.07.2012) - 13:06:40 (15.07.2012)	5.32	17.8	0.919
02.08.2012	09:20:00 - 20:26:40	1.93	19.4	0.348
05.09.2012	04:53:20 - 07:40:00	2.46	17.1	0.759

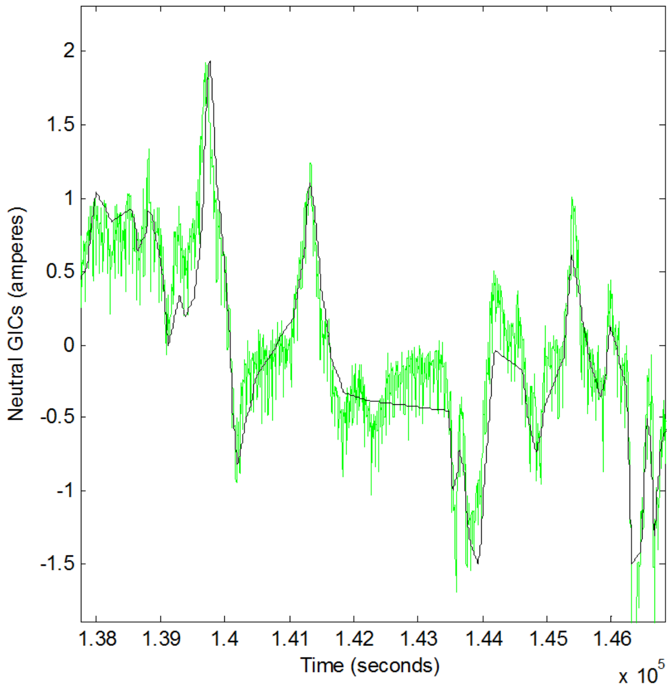

Figure 5.4: Comparison of measured GIC data (black) and estimated GIC data scaled up by an error scaling factor of 19.4 (green) for a period containing a current spike on 02.08.2012

Plots of the rescaled GIC estimations and the GIC measurements for these dates are shown in Fig. 5.4 through to Fig. 5.6. Note that the green plots are the estimated GICs scaled up by the error scaling factor for that time period and the black plots are the measured GIC data.

Some error in the time-varying GIC estimations in Fig. 5.4 through to Fig. 5.6 is expected simply due to the fact that the geoelectric field estimations used to calculate them were uniform, even though they were interpolated to the location of the current measuring device. It was therefore expected that no more than a rough correlation between the measured data and the scaled estimated data would be present. Indeed, the agreement is quite poor for the 5th of September as displayed in Fig. 5.5. However the fact that multiplying by a scaling factor leads to correlation as clear as that which is evident in Fig. 5.4 through to Fig. 5.6 shows that the estimations correlate with the measurements in general. Existence of a relatively constant error scaling factor was therefore deemed to be a safe conclusion.

One might posit that the error scaling factor increases with the severity of the geomagnetic disturbance, which would mean that the functions and tools developed in this thesis would have weak predictive power with respect to estimating the GIC distributions produced by geomagnetic events for which no measurements are

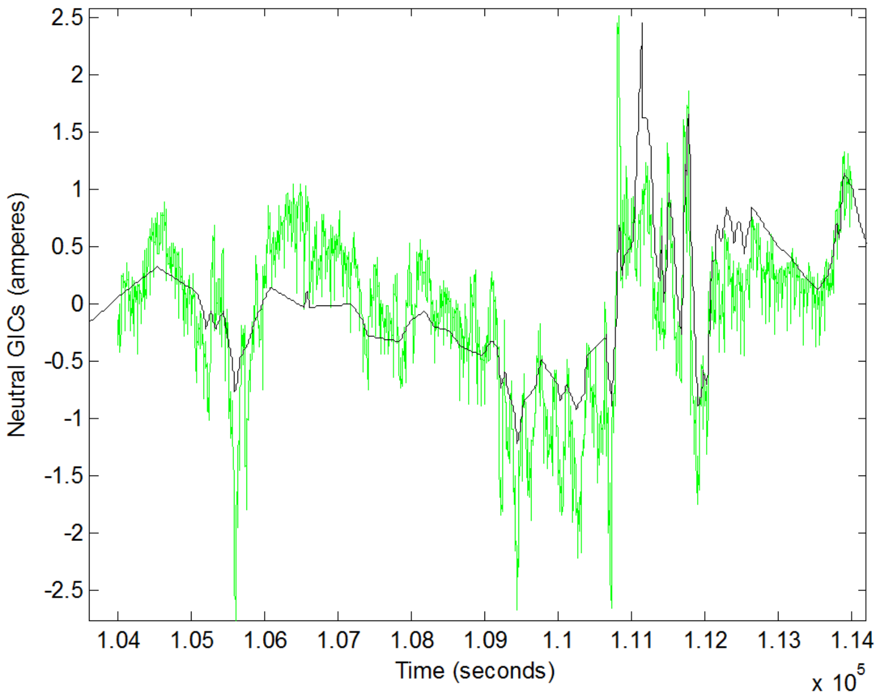

Figure 5.5: Comparison of measured GIC data (black) and estimated GIC data scaled up by an error scaling factor of 17.1 (green) for a period containing a current spike on 05.09.2012

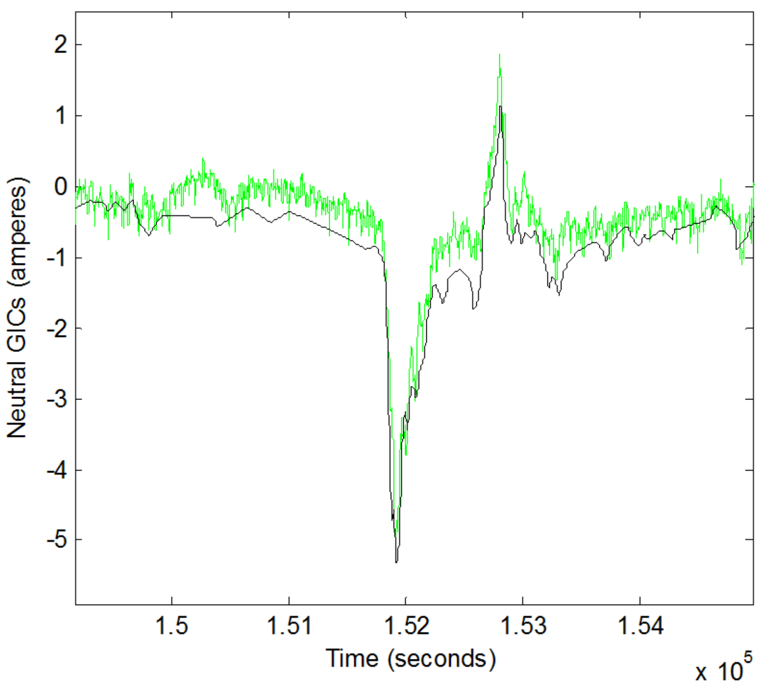

Figure 5.6: Comparison of measured GIC data (black) and estimated GIC data scaled up by an error scaling factor of 17.8 (green) for a period containing an SC on 14.07.2012

available. The values in Table 5.6 however do not indicate the existence of any such trend. It is true however that a sample of a larger number of events would have allowed better establishment of the consistency of the error scaling factor.

5.2.2 Correcting the Error Scaling Factor

Once the existence of a relatively constant error scaling factor had been determined an explanation had to be found. Apart from errors in the mfiles which were written or in spatial data, both of which were rigorously tested for and not found to be apparent, the only reasonable explanations were that the conductivity value used in calcgeoEtemporalmethod was inappropriate for Queensland, or at least for SUB901660, or that the geomagnetic coastal effect enhances GICs through TX5722392 substantially. The conductivity value chosen to represent the Earth below Queensland with a one dimensional model was adapted from the Campbell conductivity model. The first six layers of this model, as presented in [33] extend to a depth of 406.025 kilometres and the final layer extends to an infinite depth. The conductivity value used in a single-layered one dimensional model is most accurate if it is taken as a depth-weighted average over the depths to which the disturbance being studied penetrates. The skin depth δ, which denotes the depth at which a signal has been reduced by a factor of 1/e or approximately 0.3679, is a function of both the frequency of the signal and the conductivity of the Earth:

$$\delta = \sqrt{\frac{2}{\omega\mu\sigma}} \tag{5.1}$$

It should be noted that such an expression is only strictly valid for studying the penetration of an electromagnetic wave into a medium with a constant conductivity, which the Earth is not. Because the fundamental frequency of each space-weather driven geomagnetic disturbance is different it is difficult to select a single conductivity value for a single-layered one dimensional model which is applicable to all events. Though SCs can be generally expected to fall into a certain range of frequencies, not all geomagnetic disturbance events of interest are SCs. The disturbances which occurred on the 2nd of August and the 5th of September, though causing only relatively small spikes in GIC, were not related to SCs. Since no generally applicable depth of penetration could be determined it was decided that a rescaling of the Campbell conductivity model which resulted in the best agreement between estimated and measured GICs would have to be used.

In light of the fact that the most accurate conductivity value which can be chosen for a single-layered one dimensional conductivity model depends on the frequency of the disturbance it is not surprising that the error scaling factors determined for each of the 14th and 15th of July, the 2nd of August and the 5th of September were all slightly different. It is certain that in general at least some part of the error scaling factor is due to the value of conductivity chosen being inappropriate both for the frequencies of the disturbances studied and the Earth below SUB901660 and/or Queensland. The relationship between the induced geoelectric field and the Earth conductivity in Eq. (2.8) is:

$$E_y(t) \sim \frac{1}{\sqrt{\sigma}}$$

For a lower conductivity to account for all of the error therefore, the depth-weighted average conductivity calculated using the Campbell conductivity model would have to be scaled down by the inverse of the square of the error scaling factor, as follows:

$$\sigma_{scaled} = \sigma \frac{1}{19.37^2} \approx 0.00008465\ S/m$$

In [42] a 150km layer of uniform conductivity 0.001 S/m was used, with other layers beneath it, to model the Earth below the Australian continent. Smaller conductivity values are seldom found in the geomagnetic literature or surveys relevant to Queensland. Any conductivity value below 0.001 S/m, such as that which is calculated above, was therefore considered excessively small. It was apparent that a rescaling of the conductivity value used in calcgeoEtemporalmethod alone could not justify the GIC distributions estimated in this thesis.

Another source of some contribution to the error scaling factor is the geomagnetic coastal effect. In close proximity to coastlines, this phenomenon of geoelectromagnetic induction enhances the component of the induced horizontal geoelectric field perpendicular to the coastline and reduces the component parallel to the coastline. The physical origins of this phenomenon and the highly idealized and simplified method which was used in this thesis to estimate its effect on GIC distributions in the Queensland network are detailed in Sections 2.3 and 4.7.

Since one of the major feeders heading into SUB901660 is near to perpendicular to the coastline in that region, it was expected that enhancing the coastal effect should result in larger estimated GICs in the neutral of TX5722392. The coastal effect was applied during four moments when intense geoelectric fields occurred in the three time periods mentioned in Table 5.6. As expected, these calculations yielded enhanced GIC estimations for the neutral of TX5722392, and these enhanced estimations were used to calculate the re-scaled conductivity value which would be necessary to make the estimated GIC values match the measured ones. An example of this calculation for the SC which occurred on the 14th of July, for which the measured GIC was approximately -5.32 amperes and the estimated GIC with a coastal coefficient of 800 applied was approximately -1.10709 amperes, is shown below:

$$\sigma_{scaled} = \sigma \frac{1}{\left(\frac{-5.32}{-1.10709}\right)^2} = \frac{0.03176}{\left(\frac{-5.32}{-1.10709}\right)^2} \approx 0.00138\ S/m$$

It was found in general that a coastal coefficient of 800 resulted in rescaled conductivity values which were sufficiently large i.e. greater than the minimum value of 0.001 S/m used by [46]. The results for the four current spikes studied are shown in Table 5.7:

Table 5.7: Rescaled conductivity values for the moments of maximum GIC of four separate GIC spikes

Date (UTC)	Time of Current Spike (UTC)	Neutral GIC Measured During Spike (Amperes)	Rescaled Conductivity Value (Siemens/metre)
14.07.2012	18:12:23	-5.32	0.00138
15.07.2012	06:52:23	3.25	0.00168
02.08.2012	14:49:07	1.93	0.00151
05.09.2012	06:47:14	2.46	0.00178

With a coastal coefficient of 800, the distance at which the influence of the coastal effect ends is 640 kilometres inland. While this distance is likely to be in excess of the distance that the fields would actually be enhanced due to the coastal effect, the geophysical literature does not contain precise estimates of the distances inland which this effect should persist in general. In principle this distance varies with the amplitude and fundamental frequency of the geomagnetic disturbance as well as the shape of the coastline and conductivities of the Earth and seawater in the region. There are even documented regions on the Earth in the vicinity of coastlines where the coastal effect is anomalously absent [35]. It is however known in general to occur over distances on the order of hundreds of kilometres. Also, the northward and eastward fields in Fig. 5.7 are only 25% stronger than they would be in the absence of the coastline at a distance of 400 kilometres inland and 10% stronger at a distance of 500 kilometres inland.

Reducing the coastal coefficient would have resulted in more realistic maximum distances of influence of the coastal effect; however this would have also reduced

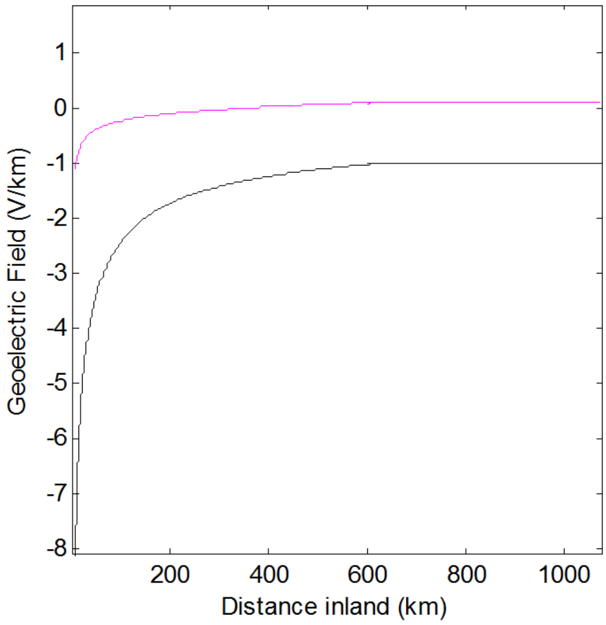

Figure 5.7: Northward geoelectric field component (pink) and eastward geoelectric field component (black) against distance inland for non-coastal geoelectric field components of 0.1V/km northward and -1V/km eastward and a coastal coefficient of 800

the rescaled conductivity values to unacceptably low levels. Increasing the coastal coefficient would have resulted in higher rescaled conductivity values but would have required that the coastal effect persisted further in land. The extent inland which the coastal effect persists when modelled with coastalgeoE, a coastal coefficient of 800 and non-coastal background fields of 1V/km westward and 0.1V/km northward is shown in Fig. 5.7.

Despite all simplifications and approximations made it was assumed that the GIC distributions generated in the Queensland network by space weather disturbances could be estimated with adequate accuracy by using a rescaled conductivity of 0.00151 S/m and a coastal coefficient of 800. The rescaled conductivity value calculated using the GIC estimations and measurements of the 2nd of August was deemed the most appropriate as it lies roughly in the middle of the other rescaled conductivities calculated. Also, the estimations for that day are known to have correlated well with the measured data as indicated by the low root mean square difference value in Table 5.6.

5.2.3 Investigating the Importance of Non-uniform Geoelectric Fields

One of the goals of this thesis was to investigate the difference between the distributions of GICs in the network which would be obtained if uniform and non-uniform geoelectric fields were used to model true geoelectric fields induced by space weather disturbances. Originally it had been intended to investigate the difference between these results for uniform fields and non-uniform fields in the absence of the coastal effect. It was found however that the coastal effect had to be assumed to play a dominant role in the non-uniform geoelectric fields induced across Queensland during space weather disturbances. An analysis of non-uniform geoelectric fields in the absence of the coastal effect would therefore have been trivial.

A comparison of the GIC distributions predicted by assuming a uniform geoelectric field and a non-uniform one with the coastal effect taken into account was performed for the SC of the 14th of July. The geoelectric field was estimated at three locations; Darwin, Townsville and Culgoora. In order to remove the small spatial integration errors described Subsection 4.4.1 of Chapter 4 from the comparison, runGICnonuniform was used to calculate the GICs in both the uniform and non-uniform geoelectric field cases. This way it was ensured that the differences between the estimations for the uniform geoelectric field and the estimations for the non-uniform geoelectric field were not a result of these errors as they were present equally in both sets of estimations.

The GICs present in the network at 18:12:23 on the 14th of July were calculated using runGICnonuniform with the coastal effect neglected and with the values of the geoelectric field components estimated to be present at Culgoora magnetometer station used for all three magnetometer sites. In other words the function was called as if the geoelectric field all across Queensland at that time had been equal to the value it was estimated to have had at Culgoora. While Townsville magnetometer is situated more appropriately within Queensland and Culgoora is in northern New South Wales, the latter has a location closer to the more critical southern end of the Queensland network which supplies the city of Brisbane and the surrounding shires. These uniform geoelectric field effective GICs were then scaled up by the error scaling factor for that date (17.8) and they will henceforth be referred to simply as the results for the uniform field.

The distribution of GICs in the network was also calculated using runGICnonuniform with the non-uniform nature of the geoelectric fields and the coastal effect taken into account. A coastal coefficient of 800 was applied and the geoelectric fields estimated at all three magnetometer stations, recalculated using calcgeoEtemporal-

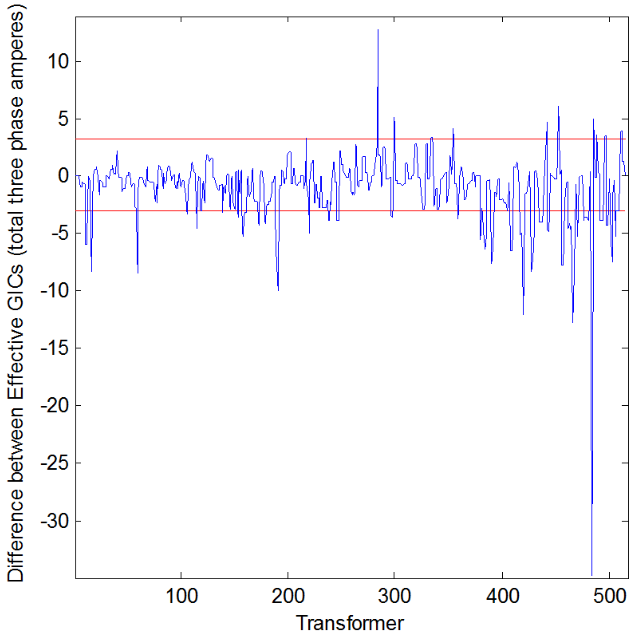

Figure 5.8: Differences in effective GIC given a uniform geoelectric field with application of an error scaling factor of 17.8 and a non-uniform geoelectric field calculated with a rescaled conductivity of 0.00151 S/m and a coastal coefficient of 800 for the SC of 14.07.2012

method and a rescaled conductivity of 0.00151 S/m, were used. These effective GIC estimations will henceforth be referred to simply as the results for the non-uniform field. The differences between the results for the uniform and non-uniform fields are plotted in Fig. 5.8.

The mean of the effective GIC estimations for the uniform geoelectric field was 3.13 amperes while the mean of the effective GIC estimations for the non-uniform geoelectric field was 2.07 amperes. The former of these and its negative have been plotted in red in Fig. 5.8 to demonstrate the significance of the differences between the uniform and non-uniform results. The differences are clearly comparable to and often greater than the mean effective GIC values. The root mean square difference between the non-uniform and uniform field results was 3.0992 amperes. In other words, if the non-uniform field results were assumed to be completely accurate, then the average error in the uniform results would be approximately 150% of the mean effective GIC value.

The conclusion drawn in Subsection 5.2.2 regarding the level of influence of the coastal effect is likely to be somewhat inaccurate; it is likely that the influence of the coastal effect should only persist for a few hundred kilometres in land at most. To confirm the importance of non-uniform geoelectric fields with more confidence,

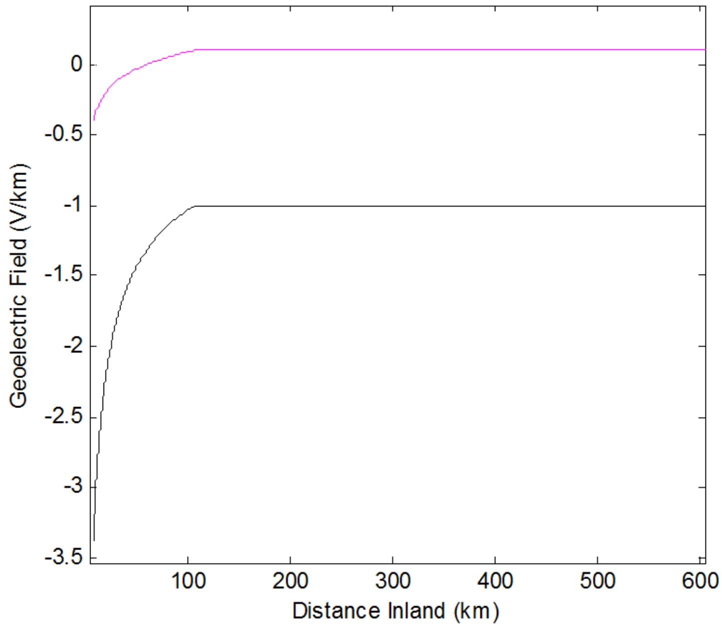

Figure 5.9: Northward geoelectric field component (pink) and eastward geoelectric field component (black) against distance inland for non-coastal geoelectric field components of 0.1V/km northward and -1V/km eastward and a coastal coefficient of 330

the above investigation was repeated with a coastal coefficient of only 330. This resulted in the coastal effect only reaching inland by approximately 100 kilometres, as shown in Fig. 5.9.

For this second investigation the uniform geoelectric field results were not multiplied by the error scaling factor. As before the geoelectric field in the uniform case was considered everywhere equal to the value estimated at Culgoora magnetometer station. The original depth-weighted average of the Campbell conductivity model, instead of the re-scaled value of 0.00151 S/m, was used in estimating the geoelectric field values at Darwin, Townsville and Culgoora for the non-uniform geoelectric field study. The differences between the uniform and non-uniform field results for this second investigation are displayed in Fig. 5.10.

The mean effective GIC value for the non-uniform field case was 0.2089 amperes and the mean effective GIC for the uniform field case was 0.1758 amperes. Again the largest of the mean effective GICs has been plotted in red to indicate the significance of the differences shown in blue. The root mean square difference between the non-uniform and uniform field results was 0.1377 amperes. If the non-uniform results were assumed to be completely accurate, then the average error in the uniform field results would be approximately 66% of the mean effective GIC value.

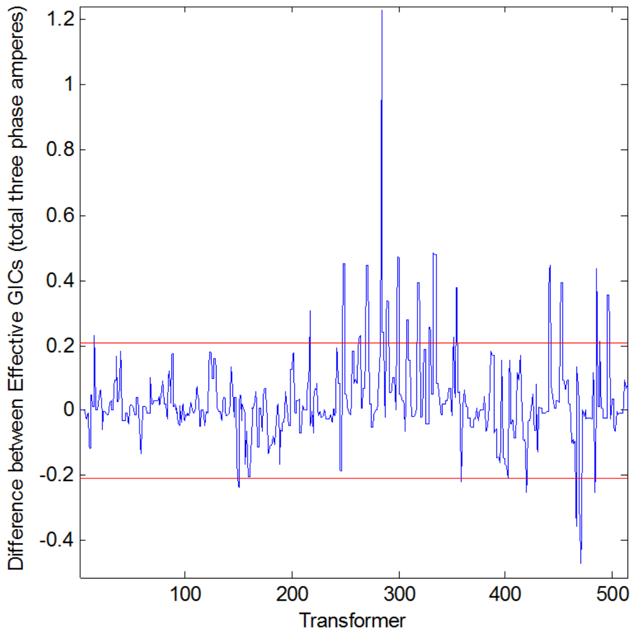

Figure 5.10: Differences in effective GIC given a uniform geoelectric field without application of an error scaling factor and a non-uniform geoelectric field calculated with a coastal coefficient of 330 for the SC of 14.07.2012

Since the coastal effect is likely to persist inland for distances longer than 100km, the second investigation in this Section demonstrates that even conservative estimates of the influence of the coastal effect result in significant differences in estimations of GIC distributions made with uniform and non-uniform geoelectric fields. It can therefore be concluded in general that using uniform geoelectric fields to estimate GIC distributions in the Queensland power transmission network, or any other network which lies in such close proximity to a coastline for such long distances, is highly inaccurate.

The transformers estimated to have the largest twenty effective GICs given the use of non-uniform geoelectric field values estimated with a rescaled conductivity value of 0.00151 S/m and a coastal coefficient of 800 are shown in Table 5.7. These are deemed to be the most accurate GIC estimations for the SC on the 14th of July.

5.3 The SC of the 24th of March 1991

On the 24th of March in 1991 an SC with an unusually short rise time occurred; plots of the H components during this event as observed at Birdsville and Weipa in Queensland are shown in Fig. 5.11. The geomagnetic data for this event was

Table 5.8: Highest twenty effective GICs estimated for the SC of the 14.07.2012 estimated using a non-uniform geoelectric field with a coastal coefficient of 800

Transformer Name	Effective Winding GIC (total three phase amperes)
TX8010757	19.2499
TX712345	15.5088
TX5324264	13.7379
TX4649542	9.9219
TX8984441	9.9219
TX8139769	9.862
TX7448678	9.4096
TX8922671	9.377
TX3414	9.3564
TX8009208	8.8895
TX1425093	8.8895
TX2322401	8.326
TX236324	8.2559
TX6074326	8.2559
TX8572127	8.1717
TX9636122	8.1717
TX9575431	7.9065
TX8928333	7.8645
TX2933679	7.8157
TX9324686	7.6811

provided by Professor K. Yumoto of Kyushu University.

The rise time of this SC was on the order of one minute, which is much shorter than the five minute rise times commonly observed of SCs. The amplitude of the disturbance to the H component exceeded 200nT at both stations making it a relatively strong SC in this respect as well.

Unfortunately a timing error had occurred during the recording of the Birdsville magnetometer station geomagnetic data; there was a time lag of approximately one minute in the data. Before geoelectric fields were estimated the Birdsville data was time-shifted back by 51 seconds in order to align the slopes of the SC in each dataset. This manipulation of the data is justified by the fact that SCs are known to occur with near simultaneity around the planet [43]. It is therefore reasonable to expect that the SC will have been observable within the space of a few seconds between

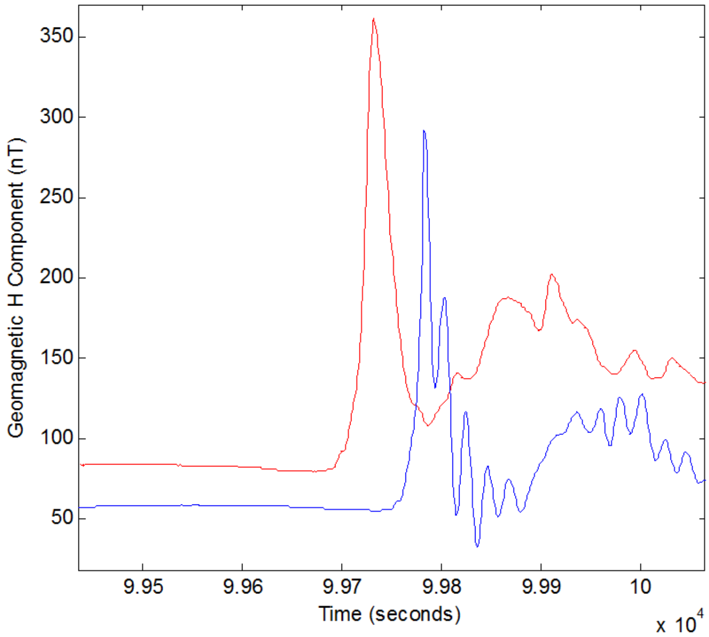

Figure 5.11: Geomagnetic H component data for the SC of 24.03.1991 measured at Birdsville (blue) and Weipa (red) magnetometer stations in Queensland

Birdsville and Weipa, which are located at the far southern and northern ends of Queensland respectively.

After time-shifting the Birdsville data the geoelectric fields generated by this SC as they would have been observed at Birdsville and Weipa were estimated using calcgeoEtemporalmethod. The GIC distribution which would have been present in the network at the moment when the geoelectric fields were most intense was then estimated using runGICnonuniform and a coastal coefficient of 800. Of course, many of the transformers included in the study were not present in the network in 1991. Many of the transmission lines in the network were also not present. The severity of GICs which actually occurred in the network is likely to have been significantly lower than those estimated here due to the fact that the smaller, less interconnected power network present in Queensland at the time may not have coupled as effectively with space weather disturbances. However the chief interest here is the effective GICs which would be present in the current network if this SC occurred today. The estimations of these ranked in ascending order are displayed in Fig. 5.12.

This SC occurred at approximately 03:41:00 UTC, which was at 1:41pm in the afternoon in AEST. The Queensland transmission network can be expected to have been fairly heavily loaded at this time of day.

For 66 of the 515 transformers included in the study the estimated effective GICs

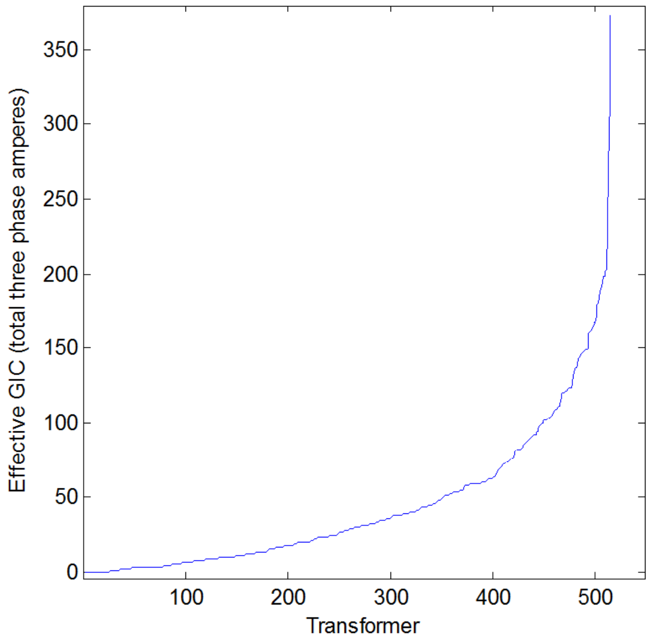

Figure 5.12: Effective GICs for the moment of maximum geoelectric field intensity during the SC of 24.03.1991 assorted in ascending order

were in excess of 100 amperes. The time interval for which GICs of this magnitude were present in the network would have been extremely brief; probably less than ten seconds. It is unlikely that significant damage could have been inflicted on transformer winding insulation or other components of transformers in such a short period of time. However the fact that effective GICs of these magnitudes could be generated in the Queensland network at all should be an important consideration in future planning for this network.

It should be noted that the effective GICs presented are total three phase GICs. The single phase GICs were a third of those presented here; this is true of all other effective GICs discussed in this thesis. However, even if they were plotted as single phase values the GICs in Fig. 5.12 would still greatly exceed those which it was previously thought could ever be present in the Queensland network.

The largest twenty effective GICs estimated for this event are shown in Table 5.8.

Table 5.9: Highest twenty effective GICs estimated for the SC of the 24.03.1991 estimated using a non-uniform geoelectric field with a coastal coefficient of 800

Transformer Name	Effective Winding GIC (total three phase amperes)
TX8010757	373.1201
TX712345	319.4094
TX5324264	273.3804
TX4649542	203.2641
TX8984441	203.2641
TX8139769	202.0371
TX7448678	198.9248
TX8922671	198.3016
TX8009208	192.056
TX1425093	192.056
TX3414	188.8006
TX2322401	180.4975
TX236324	178.9785
TX6074326	178.9785
TX2933679	171.5351
TX8572127	166.7982
TX9636122	166.7982
TX9324686	165.7966
TX3093692	161.9941
TX8928333	161.3804

5.4 The Geomagnetic Storm of the 9th of March 2012

Over the 8th and 9th of March this year a geomagnetic storm occurred which was classified as a G3 event on the NOAA Space Weather Severity Index. The geoelectric field magnitudes estimated for March the 9th using geomagnetic data recorded at the Townsville magnetometer station and a rescaled conductivity value of 0.00151 S/m are plotted in red in Fig. 5.13. Conventional wisdom when it comes to space weather suggests that significant geoelectric fields cannot be induced in mid-low latitude regions such as Queensland during geomagnetic storms other than briefly as a result of an SC. The geoelectric field magnitudes in Fig. 5.13 however, suggest otherwise. Note that the geomagnetic latitude of Townsville is approximately 26

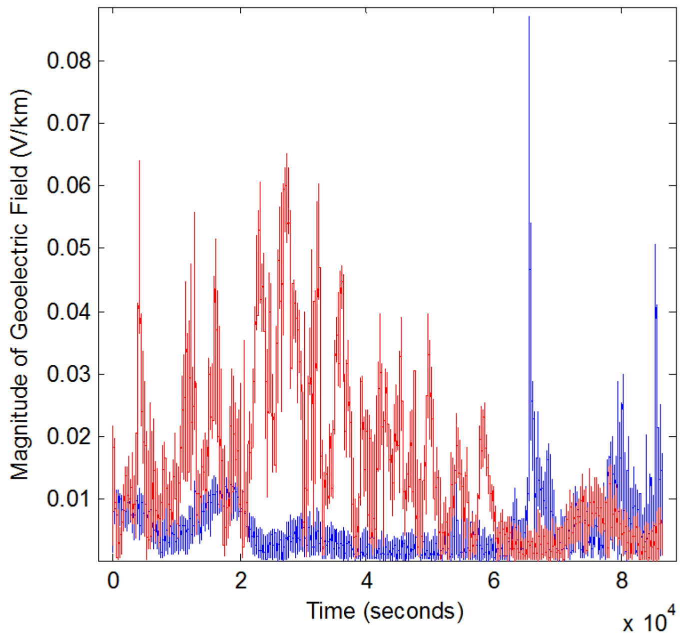

Figure 5.13: Estimated geoelectric field magnitude for 09.03.2012 (red) and 14.07.2012 (blue)

degrees south. The field strength values estimated for the SC of the 14th of July this year, also with the rescaled conductivity value, are plotted in blue for comparison. Note that this SC was estimated to have produced the GIC distribution shown in Table 5.7 in Subsection 5.2.3 of this Chapter. Note also that the coastal effect has not been applied in these calculations.

An SC did occur at the beginning of the storm over the 8th and 9th of March; however this was on March the 8th. It is therefore clear from Fig. 5.13 that several significant excursions of the geoelectric field occurred which were not associated with any SC event.

During the 9th of March the Dst index, which is an hourly-evaluated space weather index measuring the total depression of the H component of the geomagnetic field at the equator resulting from the ring current, reached magnitudes over 100nT for several hours. The most extreme value it took, as shown in Table 5.9, was -133nT at 09:00. Note that these Dst values, provided by the World Data Centre for Geomagnetism in Kyoto, are preliminary and await verification [49].

The Dst index summarizes the total energy content of the planetary ring current over one hour. The ring current is known to be populated with heightened amounts of high energy extraterrestrial plasma during geomagnetic storms due to reconnection which has occurred at the begginning of the storm. While the Dst index can

Table 5.10: Highest twenty effective GICs estimated for the SC of the 24.03.1991 estimated using a non-uniform geoelectric field with a coastal coefficient of 800

Hour	1	2	3	4	5	6	7	8	9	10	11	12
Dst	-28	-10	-19	-43	-71	-68	-77	-113	-133	-109	-113	-100
Hour	13	14	15	16	17	18	19	20	21	22	23	24
Dst	-112	-118	-110	-116	-99	-91	-83	-83	-84	-81	-74	-66

be treated as a general indicator of the severity of a geomagnetic storm it does not necessarily correspond directly to the strengh of the geoelctric fields which are produced during substorms events within that storm. Since it is related to ring current energy it is also an indicator of the number of days which a geomagnetic storm will persist for; the excess energy stored in the ring current is not necessarily released all at once.

Even given all of this, one can still expect that stronger geoelectric fields will probably be present for brief periods during geomagnetic storms of a higher maximum Dst index magnitude. The maximum Dst index magnitude on March the 9th was 133nT; this value is greatly exceeded by the maximum Dst index magnitudes of historic superstorms. In [44] it is estimated that the maximum Dst index during the superstorm of 1859, the strongest geomagnetic storm on record, was approximately -1760nT. In a recent paper [45], it is estimated that the strongest possible geomagnetic storm which could be facilitated by the balance of magnetic pressure and plasma pressure in the magnetosphere would register a Dst index of roughly -2500nT. It is clear that the possibility of strong geoelectric fields induced by the rare but exceptionally strong geomagnetic storms which are possible still needs to be investigated for power networks at all geomagnetic latitudes. Such fields are possibly of greater concern than those induced by SCs; they may be able to persist for longer periods of time than the few minutes which SC-induced geoelectric fields tend to be present for. The duration for which the power transformers in the network are subjected to GICs above a certain level effects the impact which their saturation has on the health of each of the individual machines as well as the voltage stability of the network.

Chapter 6

Limitations of the Project

A large number of factors make the results of all studies in this thesis, particularly estimations of GIC distributions made where no measurements were available, subject to various levels of inaccuracy. All results should hence be treated with appropriate levels of caution and not necessarily used for the immediate development of mitigation strategies. This Chapter should be taken into consideration before any conclusions are drawn from the results of this project.

6.1 Distribution Network Inaccuracy

Possibly the greatest cause of inaccuracy of the GIC estimations in this thesis will be the neglect of the distribution networks connected to the transmission network. This was discussed previously in Subsection 4.1.5 of Chapter 4. In reality the distributions networks will cause slight reductions in the GICs which would flow through the transmission network transformers in their absence. Relatively small voltages will be induced in their transmission lines due to them being comparatively shorter, however the transmission lines and transformers of such networks will provide alternative paths to ground for the GICs entering the substations in the transmission network.

6.2 Limitations related to the GIC Measurement Device

There are two features of the GIC measurements used in this project which limit the accuracy of the GIC estimations. The first of these is that measured data was only available for one location in the network. This limitation is significant because both the strength of the coastal effect and the conductivity of the Earth were altered so as to match estimated GICs at this location to the measured ones. If GICs had been measured at other locations in the network, the re-scalings of the coastal effect strength and Earth conductivity value which resulted in the best agreement between the GIC estimations and measurements at all locations could have been determined. The level of this agreement would indicate whether the estimation methodology was sound or whether some additional physical mechanism was missing from it.

Another limitation related to the measured GIC data was the non-ideal location of the current measurement device. The particular transformer which was chosen for application of this device was located in the middle of the network in that several major transmission lines leave from the associated substation. The neutral of the transformer which was measured is therefore a bridge between at least two parallel circuits and any inhomogenity in the error in GICs calculated in these transmission lines will have resulted in amplified error at this site. In particular the coastal coefficient and re-scaled Earth conductivity chosen using data from this site may be poor for this reason. In general one could expect that the GIC estimations might be less accurate in more complex parts of the network. If the GIC measurement device had been applied to a transformer on the edge of the network i.e. one at a substation with transmission lines from only one other substation entering it, the estimations may have been more accurate. The coastal coefficient in Eq. (4.16) and Eq. (4.17) required to match the GIC estimations to the measured data might then have been lower and more realistic.

6.3 Conductivity Model Inaccuracy

Many causes of inaccuracy in the GIC distributions estimated in this thesis stem from the inaccuracy of the assumption of conductivity inhomogeneity in one direction or another. In principle all real-world problems in electromagnetism, of which problems in the field of geoelectromagnetic induction are a subset, are three-dimensional problems. One obtains levels of analytical tractability by assuming certain geometric symmetries; if these symmetries are sufficient in one direction over the length scales of interest the problem can be approximated as one which depends on a reduced number of spatial dimensions.

In the field of geoelectromagnetic induction the source fields generated by currents in the ionosphere or magnetosphere are always assumed to be uniform since the spatial extent of these sparse but wide-reaching currents are much larger than the penetration depths of the electromagnetic disturbances they generate. This assumption is not expected to have been a source of appreciable error in this project.

In this thesis the Earth was treated as if its conductivity were invariant with both lateral position and depth. In principle of course the conductivity of the Earth is a function of both of these. The order of the inaccuracies incurred due to this approximation depend on both the severity of the lateral and vertical conductivity inhomogeneities in the Earth under Queensland and on the length scales over which these occur. For example, a river causes a small but sharp lateral and vertical conductivity inhomogeneity due to the presence of highly conductive river water. However the spatial dimensions of this environmental feature are much smaller than the penetration depths of SC and substorm disturbance fields and hence one does not expect this feature to affect the resultant surface geoelectric fields significantly. Also, the length scales of power network transmission lines are significantly greater than those of such a feature and so the affect which it has on the GICs in the transmission line running over it will be even less pronounced. The same can be said of any conductivity inhomogeneities which occur over relatively small length scales in comparison to the penetration depths of the disturbance fields and average transmission line lengths.

On the other hand, divisions between large geological structures which extend for hundreds of kilometres should presumably result in significant error when estimating geoelectric fields using a one-dimensional induction model. The Earth is of course rich with different geologic materials of different conductivities in general.

A useful method to incorporate the effects of large vertical and lateral conductivity inhomogeneities into geoelectric field estimations for the purposes of GIC studies might be to make use of apparent resistivities from magnetotelluric sounding surveys, such as those for Queensland mentioned in [46]. The apparent resistivities measured in such studies represent the weighted-average of the actual resistivity over the depths to which the test signal penetrates. The apparent resistivities measured will usually be presented in log-log plots against the period of the test signal. Selecting an appropriate resistivity value therefore requires knowledge of the fundamental frequency of the disturbance which is to be studied; this would be achievable via spectral domain analysis of the geomagnetic disturbance.

In general, two different values of apparent resistivity are calculated using measurements taken with a test signal of two distinct polarisations. Use of magnetotelluric sounding data would therefore require special resolution of the horizontal components of the geomagnetic field. The two polarisation modes are referred to as the transverse electric or TE mode and the transverse magnetic or TM mode. The former corresponds to an orientation of the test signal such that the electric field is parallel with the strike of the conductivity feature being probed and the latter an orientation where the magnetic field of the test signal is parallel to the strike of the conductivity feature. The strike of the conductivity feature is the lateral direction in which the conductivity is homogenous. Though there is no such direction for a three-dimensional conductivity feature there are methods by which to resolve such a feature into the most accurate possible approximation of a two dimensional feature. For a good explanation of all of the above, see [46].

For each location where magnetotelluric sounding data has been collected and analysed the horizontal geomagnetic field would need to be resolved into a component perpendicular with the strike of the local conductivity feature and a component parallel with it. The apparent resistivity calculated using the TE mode impedance would then be used to calculate the geoelectric field resulting from temporal variation of the former and the TM mode resistivity to calculate the geoelectric field resulting from the latter. Studies of this nature would obviously require careful collection of data from different surveys across Queensland; publications by Geoscience Australia would be a good place to begin looking for these. The calculation of geoelectric field values at locations where surveys have not been conducted would require some form of spatial interpolation between the regions for which magnetotelluric data was available.

6.4 Inaccuracy in Modelling of the Coastal Effect

Eq. (4.16) and Eq. (4.17) which were used to model the coastal effect in this thesis are obviously missing much of the physical information present in Equations (23) and (28) from [29]. These latter equations were themselves derived under grossly simplified conditions where the distance inland from the coastline is necessarily small. Study of Equation (4.162) in [39] and other expressions therein gives some idea as to the complexity of the integral equations which need to be solved to obtain solutions for two sheet models. Accurate modelling of the geoelectric fields produced in the vicinity of coastlines for a given geomagnetic disturbance would possibly require detailed two or even three dimensional induction models and high resolution numerical computation techniques such as Finite Element Analysis or Finite Difference Methods.

6.5 Span Data Inaccuracy

The span data which was collected from PLQ was found to contain some spatial disagreement errors. For some transmission lines it was necessary to assume a striaght-line path between the two substations at either end. This is not expected to have been a major source of error in this project. For more detail on this issue refer to Subsection 4.4.1 of Chapter 4.

6.6 Additional Sources of Inaccuracy

Several other factors contribute to inaccuracy of the GIC estimations made in this project for which it is unlikely that improvements could be made directly. A source of some error in this project will have been that the geomagnetic H and D components were approximated as corresponding to the geographic northward and eastward directions respectively, which is of course incorrect. The author knows however of no way to obtain the inclination of the horizontal components of the geomagnetic field at any one time, but expects that the error introduced by this assumption should be on the order of only a few degrees.

One approximation which calcgeoEspectralmethod and calcgeoEtemporalmethod both share is that they both treat the magnetometer data as if it were the original disturbance field produced by the space weather events being investigated. In principle this is also incorrect; the geomagnetic field measured includes both the field of the disturbance and the response field produced due to induction in the various layers of the Earth. Separation of measured geomagnetic data into the source field and induction fields entails methods in geomagnetic deep sounding beyond the scope of this project.

A source of error in estimating non-uniform geoelectric fields was the lack of spatial resolution provided by using only three magnetometer sites, especially when only one of these was located inside Queensland. It is possible that significant spatial variations of the fields estimated occurred which were too small to be picked up by this small system of sampling points. Additional geoemagnetic data from stations inside Queensland is also available on the Supermag website; an international collaborative effort between space weather science agencies and research groups to gather geomagnetic data. However data from this site was unfortunately not available for 2012 as it is subjected to a gradual data-verification process before it is released to the general public.

It is also true that the geoelectric fields have been estimated as if the power system itself were absent; in reality the generation of the GICs themselves will indeed change the geoelectric fields which are driving them to some extent. This change is expected to be negligible however, especially in comparison to the effect which the telluric currents flowing through the Earth have on the resultant fields. It should be noted that although the temporal domain geoelectric field estimation technique used in this thesis entails inaccuracies of several forms, it does approximately take into account the telluric currents generated during the geomagnetic disturbance under investigation.

Chapter 7

Conclusion

7.1 Project Summary

Due to the large spatial distances spanned by power transmission networks, they can couple with the low frequency disturbances known generally as geomagnetic storms. This coupling specifically entails the generation of Geomagnetically Induced Currents or GICs in the network which enter through the grounding points of the wye-windings of power transformers. GICs cause transformers to saturate magnetically which results in excess heating of the machine due to eddy currents and potential damage to the windings and winding insulation. During saturation transformers also consume excess reactive power, potentially causing voltage stability issues across entire power networks and in the worst case scenario, voltage collapse of the system.

Conventionally it has only been power utilities in countries of high latitudes which were concerned with space weather as the majority of all space weather issues in power systems have occurred in such locations. Recent research has shown however that a specific type of geomagnetic disturbance known as a Sudden Commencement or SC can generate GICs in power networks at any location in the world. It has also been demonstrated that GICs can cause cumulative damage to transformers which result in eventual failure of the machine that often goes unexplained and that this can occur in low latitude regions. Because the transformers are not rendered out of service immediately, the failure might often not have been attributed to space weather when this was in fact the predominant cause.

It has therefore become necessary to re-evaluate the vulnerability of power networks in Australia to GICs. The aims of this project were to develop a GIC estimation methodology for the Queensland power transmission network and to use it to investigate the importance of non-uniform geoelctric fields, as well as to assisst in the re-evaluation of risk. The first task in achieving these aims was to collect network data and develop code to calculate the distribution of GICs in the network given known geoelectric fields. This was then to be used to calculate what the distribution of GICs in the network for a 1V/km uniform westward and northward geoelectric field would be; this was accomplished. It was recognised that the geoelectric fields induced across Queensland during SCs tend to have westward components an order of magnitude stronger than their northward components; the results for the uniform westward field should therefore be treated as more important for the Queensland network.

It was found that while the Queensland power transmission network has a greater span from north to south than it does from east to west, a uniform geoelectric field with a magnitude of 1V/km does not generate a significantly different level of GICs in the network on average if it has a northward orientation than if it has an eastward orientation. Another interesting finding of the uniform fields study was that removal of four relatively long feeders with predominantly east-west orientations from the network failed to reduce the average magnitudes of GIC in the network given a uniform westward geoelectric field.

The second major task of this project was to estimate the GIC distributions caused in the network based on geoelectric fields estimated from temporal geomagnetic data and to verify these estimations against GICs measured by a transducer installed on the neutral of a transformer at SUB901660. The estimated GICs were found to correlate well with the measurements but to be out by a fairly consistent scaling factor. This scaling factor was fond to have a value of roughly 17-19 via investigation of three separate events.

It was concluded that some of this error was attributable to inappropriateness of the conductivity value used for the Earth beneath Queensland and some of it was attributable to enhancement of the geoelectric fields due to the geomagnetic coastal effect. The geomagnetic coastal effect is the enhancement of the geoelectric fields induced across the Earth during space weather disturbances over what they would normally be due to the sharp lateral conductivity in-homogeneities presented by coastlines. A highly idealized and approximated model was developed to try to incorporate the influence of the coastal effect on the GIC distribution in the Queensland power network into the GIC estimations. This was used to determine an appropriate coefficient to regulate the strength of this effect and an appropriate rescaling of the conductivity value used. It should be understood that these re-scalings, both of the Earth conductivity value and the strength of the coastal effect, were decided upon based on measured data from only one location and are therefore possibly highly inaccurate. The strength which was assigned to the coastal effect is likely to be too high in any case.

Following these investigations, the GIC distribution which was present in the network during the SC of the 14th of July 2012 was estimated with both a uniform and a non-uniform geoelectric field. The results of these were compared and used to demonstrate the importance of non-uniform geoelectric fields in calculating GIC distributions in power networks. It was concluded that despite the relative uniformity of disturbances to the geomagnetic field produced by SCs in mid-low latitude regions, basing estimations of GICs in power transmission networks in such regions on uniform geoelectric fields is highly inaccurate in general.

The GIC estimation methodology developed was also used to estimate the GICs which would be present in the Queensland network if the unique and powerful SC of March 24 1991 occurred today. For the largest of these the effective GIC was approximately 373 amperes. The effective GICs of 66 of the 515 transformers in the study exceeded 100 amperes. Although these currents would only be present in the network for a matter of seconds due to the exceptional sharpness of this SC, the fact that GICs of this magnitude could be generated in the Queensland network defies conventional wisdom when it comes to space weather and raises the need for further investigation of this issue.

The geoelectric fields induced at Townsville during the G3 level geomagnetic storm which occurred on March 9 of 2012 were also calculated and the preliminary values of the Dst index for that day were compared to those which have occurred in historic superstorms. The fact that geoelectric fields of non-trivial magnitudes which were not related to any SC event were present on that day should also be a justification for the relevance of this issue to Australian power utilities in the future.

7.2 Recommendations for Future Work

There are several alleyways of improvement for the GIC estimation methodology used in this thesis. Also, some of the investigations in Chapter 5 could be pursued further as interesting research questions in their own right. They could be investigated using large IEEE standard bus systems and commercial software which solve GIC distributions given specified geoelectric fields such as PowerWorld Simulator. There are several common notions regarding the properties of distributions of GICs in large power networks which may or may not be accurate in general.

The first of these was challenged in Subsection 5.1.1 of Chapter 5; that the orientation of a uniform geoelectric field should significantly change the average effective GIC in the transformers of the network. One would expect that a northward geoelectric field would produce a higher level of GICs on average in the Queensland power transmission network as this network undoubtedly spans a greater distance from north to south than from east to west. The influence of geoelectric field orientation on the average effective GIC in a power network which has a significantly greater total transmission line length in one direction than the other should be further investigated.

The second notion that has been challenged is that removal of a few relatively long transmission lines with predominantly east-west orientations should reduce the level of GICs in the network overall given a uniform westward or eastward geoelectric field. Contingency analyses could easily be conducted to further investigate this property of large power networks in general. It would also be interesting to investigate the existence of a critical point general to all large power networks which marks a change in the trend of average effective GIC as a result of the number of east-west feeders removed.

Also an interesting question to pursue would be the increase in GIC-estimation accuracy which could be achieved via use of magnetotelluric survey data in geoelectric field estimations, as was discussed in Section 6.3 of Chapter 6. Studies which could achieve this however would probably require the use of several GIC measurement devices spread across a large power network so that multiple sets of measured data could be used to confirm the accuracy of the two-dimensional conductivity model developed. Wherever possible the measurement devices should be applied to transformers on the edge of the network i.e. at substations with major transmission lines entering from only one direction.

As mentioned in Section 6.2, accurate modelling of the influence of the geomagnetic coastal effect on GIC distributions in power networks may require detailed two or even three dimensional modelling using computational techniques to numerically approximate the integral equations which must be solved. Such techniques may include Finite Element Analysis or Finite Difference methods. The power engineering community lacks the ability to conduct such studies on its own. There must therefore be collaboration between the geophysical community and the power industry to improve predictive capabilities with respect to GIC distributions in power networks close to coastlines. Indeed; similar communication also needs to be established between the space weather physics community and the power industry to facilitate efficient communication of developments in space weather forecasting.

Finally, the accuracy of the GIC estimation methodology used in this thesis could be significantly improved if network data pertaining to the distribution networks were also included in the study.

7.3 Final Comments

The GIC estimations produced in this project are likely to contain several forms of inaccuracy, as was discussed in detail in Chapter 6. As such, they should not be used for the immediate development of mitigation strategies; the geoelectric fields and GIC distributions estimated in this thesis should be considered no more than preliminary results.

The two most interesting theoretical results presented in thesis are that non-uniform geoelectric fields must be used to calculate GIC distributions accurately in large power networks which are situated in close proximity to coastlines and that effective GICs of hundreds of amperes can be excited in power networks in mid-low latitude regions by SCs. Both of these results are accurate despite all limitations of the project. The differences between the effective GIC estimations for a uniform and a non-uniform geoelectric field were still significant in comparison to the average effective GIC when the non-uniform field was based on a highly conservative value of the coastal coefficient. As for the effective GICs estimated for the SC of March 24 1991, the limitations of this project will mean that the distribution of GICs will be inaccurate. Given the size of the power network however and the fact that the GIC estimation methodology was based mostly on physical laws with some alteration of unknown parameters to match estimations to measurements, it can at least be assumed that the order of magnitude of the largest of these GICs is a reliable result.

The methodology for estimating GIC distributions presented in this thesis should hopefully encourage future studies which improve upon it. As discussed previously, this methodology could be greatly improved upon if measured GIC data from devices installed at several locations in a large power network were available. Other improvements to the methodology could include using a two dimensional conductivity model derived from magnetotelluric survey data, including network data pertaining to the distribution systems in the study and using powerful computational techniques to estimate the influence of the coastlines on the geoelectric fields present during space weather events.

Above all this thesis should serve as a call for collaboration between all types of companies in the power industry and the space weather physics and geophysics communities in dealing with space weather issues.

Bibliography

[1] R. Pirjola, “Geomagnetically induced currents during magnetic storms,” in *IEEE Transactions on Plasma Science*, NEW YORK, pp. 1867-1873.

[2] R. Pirjola, L. Chun-ming, and L. Lian-guang, “Geomagnetically Induced Currents in electric power transmission networks at different latitudes,” in *Electromagnetic Compatibility (APEMC), 2010 Asia-Pacific Symposium on*, 2010, pp. 699-702.

[3] P. R. Price, “Geomagnetically induced current effects on transformers,” *Power Delivery, IEEE Transactions on*, vol. 17, pp. 1002-1008, 2002.

[4] J. G. Kappenman and V. D. Albertson, “Bracing for the geomagnetic storms,” *Spectrum, IEEE*, vol. 27, pp. 27-33, 1990.

[5] W. A. Radasky and J. G. Kappenman, “Impacts of geomagnetic storms on EHV and UHV power grids,” in *Electromagnetic Compatibility (APEMC), 2010 Asia-Pacific Symposium on*, 2010, pp. 695-698.

[6] B. Bozoki, S. R. Chano, L. L. Dvorak, W. E. Feero, G. Fenner, E. A. Guro, C. F. Henville, J. W. Ingleson, S. Mazumdar, P. G. McLaren, K. K. Mustaphi, F. M. Phillips, R. V. Rebbapragada, and G. D. Rockefeller, “The effects of GIC on protective relaying,” *IEEE Transactions on Power Delivery*, vol. 11, pp. 725-739, 1996.

[7] T. S. Molinski, “Why utilities respect geomagnetically induced currents,” *Journal of Atmospheric and Solar-Terrestrial Physics*, vol. 64, pp. 1765-1778, 2002.

[8] D. A. Gurnett and A. Bhattacharjee, Introduction to plasma physics: with space and laboratory applications. New York: Cambridge University Press, 2005.

[9] G. Schubert, “Magnetospheric Contributions to the Terrestrial Magnetic Field,” ed: *Elsevier Science* [Imprint], 2007, pp. 77-92.

[10] D. Rees, "Observations and Modeling of Ionospheric and Thermospheric Disturbances during Major Geomagnetic Storms - a Review," *Journal of Atmospheric and Terrestrial Physics*, vol. 57, pp. 1433-1433, 1995.

[11] M. A. Abdu, "Major phenomena of the equatorial ionosphere-thermosphere system under disturbed conditions," *Journal of Atmospheric and Solar-Terrestrial Physics*, vol. 59, pp. 1505-1519, 1997.

[12] J. G. Kappenman, "Storm sudden commencement events and the associated geomagnetically induced current risks to ground-based systems at low-latitude and midlatitude locations," *Space Weather*, vol. 1, p. 1016, 2003.

[13] L. Chun-Ming, L. Lian-Guang, and R. Pirjola, "Geomagnetically Induced Currents in the High-Voltage Power Grid in China," *Power Delivery, IEEE Transactions on*, vol. 24, pp. 2368-2374, 2009.

[14] A. Shinbori, T. Ono, M. Iizima, A. Kumamoto, and Y. Nishimura, "Enhancements of magnetospheric convection electric field associated with sudden commencements in the inner magnetosphere and plasmasphere regions," *Advances in Space Research*, vol. 38, pp. 1595-1607, 2006.

[15] S. Fujita, T. Tanaka, T. Kikuchi, K. Fujimoto, K. Hosokawa, and M. Itonaga, "A numerical simulation of the geomagnetic sudden commencement: 1. Generation of the field-aligned current associated with the preliminary impulse," *Journal of Geophysical Research-Space Physics*, vol. 108, 2003.

[16] A. Pulkkinen, A. Thomson, E. Clarke, and A. McKay, "April 2000 geomagnetic storm: ionospheric drivers of large geomagnetically induced currents," *ANNALES GEOPHYSICAE*, vol. 21, pp. 709-717, 2003.

[17] R. A. Marshall, E. A. Smith, M. J. Francis, C. L. Waters, and M. D. Sciffer, "A preliminary risk assessment of the Australian region power network to space weather," *SPACE WEATHER-THE INTERNATIONAL JOURNAL OF RESEARCH AND APPLICATIONS*, vol. 9, 2011.

[18] H. Nevanlinna, "A study on the great geomagnetic storm of 1859: Comparisons with other storms in the 19th century," *Advances in Space Research*, vol. 38, pp. 180-187, 2006.

[19] M. Lahtinen and J. Elovaara, "GIC occurrences and GIC test for 400 kV system transformer," *Power Delivery, IEEE Transactions on*, vol. 17, pp. 555-561, 2002.

[20] R. A. Walling and A. H. Khan, “Characteristics of Transformer Exciting-Current during Geomagnetic Disturbances,” *IEEE Transactions on Power Delivery*, vol. 6, pp. 1707-1714, 1991.

[21] D. H. Boteler, R. J. Pirjola, and H. Nevanlinna, “The effects of geomagnetic disturbances on electrical systems at the Earth’s surface,” *Advances in Space Research*, vol. 22, pp. 17-27, 1998.

[22] N. Takasu, T. Oshi, F. Miyawaki, S. Saito, and Y. Fujiwara, “An Experimental-Analysis of Dc Excitation of Transformers by Geomagnetically Induced Currents,” *IEEE Transactions on Power Delivery*, vol. 9, pp. 1173-1173, 1994.

[23] T. K. Saha, “Review of modern diagnostic techniques for assessing insulation condition in aged transformers,” in *IEEE Transactions on Dielectrics and Electrical Insulation*, PISCATAWAY, pp. 903-917.

[24] C. T. Gaunt and G. Coetzee, “Transformer failures in regions incorrectly considered to have low GIC-risk,” in *Power Tech, 2007 IEEE Lausanne*, 2007, pp. 807-812.

[25] S. Lu and Y. Liu, ”FEM analysis of DC saturation to assess transformer susceptibility to geomagnetically induced currents,” in *IEEE Transactions on Power Delivery, NEW YORK*, pp. 1367-1376.

[26] Lehtinen, M, Pirjola, and G. R, “Currents produced in earthed conductor networks by geomagnetically-induced electric fields” vol. 3. Paris, FRANCE: Gauthier-Villars, 1985.

[27] R. Pirjola, “Fundamentals about the flow of geomagnetically induced currents in a power system applicable to estimating space weather risks and designing remedies,” *Journal of Atmospheric and Solar-Terrestrial Physics*, vol. 64, pp. 1967-1972, 2002.

[28] D. H. Boteler and R. J. Pirjola, “Modelling geomagnetically induced currents produced by realistic and uniform electric fields,” *IEEE Transactions on Power Delivery*, vol. 13, pp. 1303-1308, 1998.

[29] J. L. Gilbert, “Modeling the effect of the ocean-land interface on induced electric fields during geomagnetic storms,” *Space Weather- The International Journal of Research and Applications*, vol. 3, 2005.

[30] C. M. Ngwira, “Geomagnetically induced current characteristics in southern Africa,” 2009.

[31] A. Pulkkinen, R. Pirjola, and A. Viljanen, “Determination of ground conductivity and system parameters for optimal modeling of geomagnetically induced current flow in technological systems,” *Earth Planets and Space*, vol. 59, pp. 999-1006, 2007.

[32] R. Pirjola, “Effects of space weather on high-latitude ground systems,” *Advances in Space Research*, vol. 36, pp. 2231-2240, 2005.

[33] R. A. Marshall, C. L. Waters, M. D. Sciffer, “Spectral Analysis of pipe-to-soil potentials with variations of the Earths magnetic field in the Australian region”, *Space Weather*, vol. 8, 2010.

[34] K. Yumoto and the 210MM Magnetic Observation Group, “The step 210 Magnetic meridian network Project”, *Journal of geomagnetism and geoelectricity*, vol. 48, pp. 1297-1309, 1996.

[35] W. D. Parkinson and F. W. Jones, “The geomagnetic coast effect,” *Rev. Geophys.*, vol. 17, pp. 1999-2015, 1979.

[36] T. Araki, “A Physical Model of the Geomagnetic Sudden Commencement”, *Solar Wind Sources of Magnetospheric Ultra-Low-Frequency Waves*, Geophysical Monograph 81., pp. 183-200, 1994.

[37] A. Shinbori, Y. Tsuji, T. Kikuchi, T. Araki, and S. Watari, “Magnetic latitude and local time dependence of the amplitude of geomagnetic sudden commencements,” *J. Geophys. Res.*, vol. 114, p. A04217, 2009.

[38] A. Viljanen and R. Pirjola, “Statistics on geomagnetically-induced currents in the Finnish 400 kV power system based on recordings of geomagnetic variations,” *Journal of geomagnetism and geoelectricity*, vol. 41, p. 411, 1989.

[39] J. T. Weaver, Mathematical methods for geo-electromagnetic induction. Taunton, Somerset, England: Wiley, 1994.

[40] J. Grainger, Power system analysis. New York: McGraw Hill, 1994.

[41] W. H. Campbell, “Quiet-day ionospheric currents and their application to upper mantle conductivity in Australia,” *Earth, planets, and space*, vol. 50, p. 347, 1998.

[42] L. J. Wang and F. E. M. Lilley, “Inversion of magnetometer array data by thin-sheet modelling,” *Geophysical Journal International*, vol. 137, pp. 128-138, 1999.

[43] T. Kikuchi and T. Araki, "Horizontal transmission of the polar electric field to the equator," *Journal of Atmospheric and Terrestrial Physics*, vol. 41, pp. 927-936, 1979.

[44] B. T. Tsurutani, "The extreme magnetic storm of 12 September 1859," *Journal of geophysical research*, vol. 108, p. 1268, 2003.

[45] V. M. Vasylinas, "The largest imaginable magnetic storm," *Journal of Atmospheric and Solar-Terrestrial Physics*, vol. 73, pp. 1444-1446, 2011.

[46] Lilley, M. F. E, Wang, J. L, Chamalaun, H. F, Ferguson, and G. I. J, Carpentaria Electrical Conductivity Anomaly, Queensland, as a major structure in the Australian plate. Boulder, CO, ETATS-UNIS: Geological Society of America, 2003.

[47] Website of the Ionospheric Prediction Service, last accessed 28.09.2012, URL: http://www.ips.gov.au/World_Data_Centre/1/2

[48] Website of GeoScience Australia, last accessed 03.08.2012, URL: http://www.ga.gov.au/

[49] Website of the World Data Centre for Geomagnetism, Kyoto, last accessed 14.08.2012, URL: http://wdc.kugi.kyoto-u.ac.jp/dst_realtime/201203/index.html

[50] S. Tsunomura, "Characteristics of geomagnetic sudden commencement observed in middle and low latitudes," *Earth Planets Space*, vol. 50, pp. 755772, 1998.

[51] K. Fox (2012, April 16), "Giant Prominence Erupts", [Online] Available: http://www.nasa.gov/mission_pages/sunearth/news/News041612-M1.7flare.html

[52] K. Zheng, D. H. Boteler, R. Pirjola, L. G. Liu, R. Becker, L. Marti, S. Boutilier and S. Guillon, "Influence of System Characteristics on the Amplitudes of Geomagnetically Induced Currents," unpublished.